January 2013

Understanding Transport Variability of the Antarctic Circumpolar Current Using Ocean Bottom Pressure

Jessica Makowski
University of South Florida, jmakowski@mail.usf.edu

Understanding Transport Variability of the Antarctic Circumpolar Current Using Ocean Bottom Pressure

by

Jessica K. Makowski

A thesis submitted in partial fulfillment
of the requirements for the degree of
Master of Science
Department of Physical Oceanography
College of Marine Science
University of South Florida

Major Professor: Don P. Chambers, Ph.D.
Gary Mitchum, Ph.D.
Sang-Ik Shin, Ph.D.

Date of Approval:
October 21, 2013

Keywords: Antarctic Circumpolar Current, Southern Ocean, GRACE, Ocean Bottom Pressure, Ocean Transport

Dedication

To one of the strongest and most independent women I had the pleasure to learn from. Thank you for being one of the reasons I am who I am today and for always encouraging me to pursue my goals. Wish you were here to celebrate with me. Love to you, a bushel and a peck.

Acknowledgments

Many thanks to my committee members, Don Chambers, Gary Mitchum, and Sang-Ik Shin, for their support and suggestions with my research. Especially my advisor, Don, who took a chance bringing in a biologist and somehow turned me into a physicist. Many thanks to all those involved in my project and research (even in the smallest of ways), your assistance and guidance when working through problems, especially programming, are very much appreciated. To all my friends for their patience and encouragement, for being there through tough times, and continuing to support my stubborn goal of completing graduate school. Finally, to my family, through all of the trials and tribulations we've had these last three years, I would be nowhere without you all.

Contents

List of Tables

List of Figures

Abstract

Previous studies have suggested that ocean bottom pressure (OBP) can be used to measure the transport variability of the Antarctic Circumpolar Current (ACC). The OBP observations from the Gravity Recovery and Climate Experiment (GRACE) are used to calculate transport along the choke point between Antarctica and Australia. Statistical analysis will be conducted to determine the uncertainty of the GRACE observations using a simulated data set.

There has been some evidence to suggest that Southern Hemisphere winds and the Southern Annular Mode (SAM) or the Antarctic Oscillation (AAO) play a significant role in accelerating/decelerating ACC transport, along with some contribution from buoyancy forcing. We will examine whether average zonal wind stress, wind stress curl, local zonal winds, or the SAM are representative of the low frequency zonal mass transport variability.

Preliminary studies suggest that seasonal variation in transport across the Australia-Antarctica choke point is driven by winds along and north of the northern front of the ACC, the Sub Tropical front (STF). It also appears that interannual variations in transport are related to wind variations centered south of the Sub Antarctic Front (SAF). We have observed a strong negative correlation/positive correlation across the STF of the ACC in the Indian Ocean, which suggests wind stress curl may also be responsible for transport variations.

Chapter 1

Introduction

The Southern Ocean has long been an under-sampled region of the world's oceans, due to its remote location. However, its dynamics play a significant role in the meridional overturning circulation, global climate system, deep water formation, and the carbon cycle (*Meredith et al.*, 2011). The Antarctic Circumpolar Current (ACC) is the defining oceanographic feature of this important ocean basin: it is the only ocean current that is not constrained by any land mass to the east at the Drake Passage and it has measurable currents to the bottom. There are still many unanswered questions concerning the ACC transport. For example, the amplitude and dominant periodicities of the ACC transport are largely unknown, especially at periods longer than one year, and it is unclear how the ACC will be affected by a changing global climate. These questions remain in large part due to the difficulties inherent in sampling polar regions. Strong seasonality and harsh ocean conditions have limited most of the *in situ* observations of major physical parameters (e.g., temperature, salinity, velocity, ocean bottom pressure, sea level) to a few warm season transects across the Drake Passage and south of Australia and in other areas with more infrequent measurements (e.g., *Rintoul and Sokolov*, 2001; *Cunningham et al.*, 2003; *Böning et al.*, 2008). From these data it has been shown that the ACC is comprised of three to four major fronts (depending on the location) and that the mean transport of the ACC can be determined to within 10-15 Sverdrup (Sv, 1 Sv = 10^6 m^3/s) (e.g., *Cunningham et al.*,

2003). The data have also shown that the transport of the ACC can vary quite a bit from month to month, but the sampling is insufficient for determining low-frequency variations. The purpose of this work is to improve understanding of ACC transport variability by using ocean bottom pressure (OBP) variations. These OBP variations are derived from satellite measurements of time-variable gravity made by the Gravity Recovery and Climate Experiment (GRACE) and will be used to quantify monthly variations in the ACC transport south of Australia from 2003 until 2012.

1.1 Dynamics of the Antarctic Circumpolar Current

The ACC is driven by the balance of strong Southern Hemisphere (SH) westerlies and friction with a complex bottom topography. There are four major fronts of the ACC: the Sub-Tropical Front (STF), the Polar Front (PF), the Sub-Antarctic Front (SAF), and the Southern ACC Front (SACCF). These were initially observed individually from repeat hydrographic sections (e.g., *Deacon*, 1937; *Nowlin and Klinck*, 1986). *Orsi et al.* (1995) quantified their approximate locations globally (Figure 1.1), using all available temperature data from the World Ocean and Climate Experiment (WOCE). However, a more recent study by *Sokolov and Rintoul* (2009) suggests that the front positions are dynamic and may have shifted by up to 1° degree south of those defined by *Orsi et al.* (1995).

The STF forms a strong northern boundary in the Indian Ocean, but is only weakly defined in the Pacific and does not pass through the Drake Passage (Figure 1.1). This means that there is mass transported into the Pacific that does not leave through the Drake Passage, but must be returned to the Indian Ocean via the Indonesian Throughflow (*Lee et al.*, 2002). *Cunningham et al.* (2003) determined the mean total transport through the Drake Passage to be 136.7±7.8 Sv (one stan-

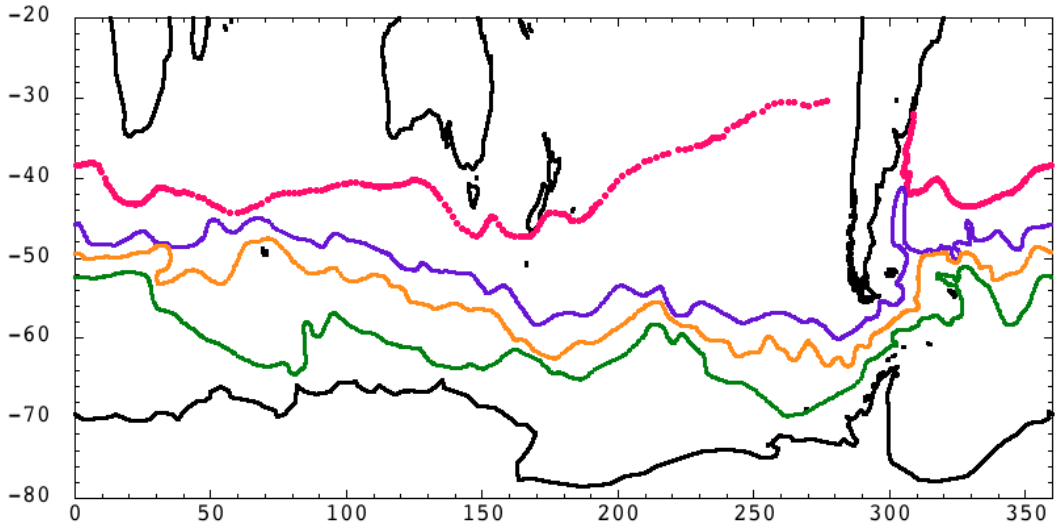

Figure 1.1: Map of front positions from *Orsi et al.* (1995). The four major fronts, the Sub-Tropical Front (pink), Sub-Antarctic Front (purple), Polar Front (orange), and the Southern ACC Front (green), are plotted based on the *Orsi et al.* (1995) front positions.

dard deviation). The mean total transport through the Australian-Antarctica choke point, measured using repeat hydrographic sections by *Rintoul and Sokolov* (2001), is 147±10 Sv (one standard deviation). The mean transports of all of the fronts as observed by the repeat hydrographic sections from the *Rintoul and Sokolov* (2001) and *Cunningham et al.* (2003) studies are summarized in Table 1.1. The approximate mean transport of the STF (∼10 Sv) is inferred from the difference between the Australian-Antarctica choke point transport (*Rintoul and Sokolov*, 2001) and the transport through the Drake Passage (*Cunningham et al.*, 2003) and is consistent with model estimates (*Lee et al.*, 2002). The majority (>90%) of the ACC transport is along the Polar and Sub-Antarctic Fronts.

One of the first studies to discuss potential mechanisms for the ACC was done by *Munk and Palmen* (1951). They argued that due to the lack of lateral boundaries along the length of the ACC, because of the Drake Passage, the wind stress must be balanced by bottom friction, mainly at major submarine ridges. *Nowlin and Klinck*

Table 1.1: Mean transports of the four major fronts in the ACC. Transport for the SACCF, PF, and SAF are described by *Cunningham et al.* (2003), and the transport for the STF is inferred from the difference between mean total transport from *Cunningham et al.* (2003) and *Rintoul and Sokolov* (2001).

Front	Transport (Sv)
Southern ACC Front (SACCF)	9.3±2.4
Polar Front (PF)	57.5±5.7
Sub-Antarctic Front (SAF)	53±10
Sub-Tropical Front (STF)	∼10
Total ACC Transport	147±10

(1986) looked at the balance of forces of the ACC with a model. However, they were unable to examine all of the potential mechanisms due to the low resolution of the model. Instead, they looked at smaller regions of the ACC with combined dynamics or reduced dynamics and suggested that future studies focus on the relative contributions of wind forcing, buoyancy fluxes, topography, and dynamic instabilities to ACC transport. Since those beginning studies, which tended to focus on the entire ACC, there has been more attention paid to the Drake Passage, where data are more frequent. *Meredith et al.* (2011) have recently reviewed the numerous investigations that looked into the balance of forces in the ACC, and concluded that the prevailing mechanism underlying the mean transport is wind stress balanced by bottom form drag. However, there is evidence that variability in the transport at the Drake Passage may be related to wind stress curl in the latitude bands north of the Drake Passage which will cause meridional mass movement, altering the pressure gradients across the ACC, as well as changing buoyancy forcing south of the ACC. These relationships, however, have only been confirmed on subannual periods. There is also evidence that the mean transport along the STF is likely driven more by Sverdrup balance

north of 55°S. *Mestas-Nuñez et al.* (1991) showed that the barotropic transport was in equilibrium with the wind stress curl north of 55°S, the northern boundary of the Drake Passage.

Nowlin and Klinck (1986) found that transport varied by up to 20% of the mean (∼20 Sv) and that most of this was caused by changes in the current at 2500 m rather than changes in the vertical shear. This is a significant problem in measuring transport variability, since temperature and salinity have not routinely been measured below 1000-2000 m depth and a zero velocity is assumed at that depth to estimate geostrophic currents. There are, however, significant currents below 2000 m in the ACC that continue to the seafloor. *Cunningham et al.* (2003) compared transport measurements assuming a zero velocity at 2500 m to transport calculated using currents measured at the deepest cast along six transects of the Drake Passage. Their results show that there is a large contribution to the transport and its variability from the currents below 2500 m (*Cunningham et al.*, 2003). Errors are as large as 50 Sv. That study emphasizes the potential for a strong contribution from small, but deep currents in the variability of the ACC and the importance of accounting for these in the calculation. The limitation of the *Cunningham et al.* (2003) study is the ability to conduct measurements for an extended period of time (e.g., a decade or more) and at regular intervals (e.g., monthly). This type of *in situ* analysis can also only be conducted during the summer months, again limiting the amount of data available for other times of the year. This also limits the ability to understand whether the apparent change from year to year is a low-frequency signal or aliasing of high-frequency variability.

Many questions remain about the amplitude and periodicity of ACC transport variability, especially how it may respond to a warming climate. Since the ACC is driven by strong Southern Hemisphere westerlies, a change in location and strength of these winds could result in either a strengthening of the ACC transport, an increase

in the overall eddy energy without a corresponding change in the transport from the current, or a combination of these. Changes in the heat fluxes and fresh water input on the south side could cause density changes that may or may not compensate for wind changes, or could reinforce them. Direct measurements of transport from top-to-bottom hydrographic sections that include current measurements at depth are too sparse to measure anything other than a snapshot for a week or so. These types of measurements are generally repeated only after several years, so many investigations on these hypotheses have utilized model simulations.

Fyfe and Saenko (2006) used 12 different large-scale global climate models (GCMs) to simulate Southern Ocean circulation and Southern Hemisphere wind changes in response to a warming climate. Their study, based on simulated SH winds from a GCM and those from the National Centers for Environmental Prediction (NCEP) and European Centre for Medium-Range Weather Forecasting (ECMWF) 40 year reanalysis (ERA40), suggest a poleward shift and strengthening of SH winds (*Fyfe and Saenko*, 2006). An earlier study found that such a shift and strengthening would cause an increase in the transport of the ACC (*Saenko et al.*, 2005). It should be noted, however that the GCM winds were positioned 4° north of the NCEP and ERA40 observed winds and were weaker, suggesting that the "poleward shift" and strengthening of the GCM winds is merely the model winds equilibrating to actual conditions from poor initial conditions (Figure 2 in *Fyfe and Saenko* (2006)).

Experiments with eddy-resolving models find that increasing westerlies in the Southern Ocean lead to more energetic eddy variability, but no significant trends in transport through the Drake Passage (*Hallberg and Gnanadesikan*, 2006). A more recent study by *Graham et al.* (2012) used a high-resolution, coupled climate model with improved representation of horizontal gradients in temperature and salinity across the Southern Ocean. They found that the position of the Sub-Tropical front is mainly controlled by the Southern Hemisphere winds, whereas the positions of the SAF, PF,

and SACCF are controlled by topography. This suggests that the southern three fronts of the ACC are not expected to vary position as SH winds shift south, and as a result the ACC would either widen or narrow as the STF shifted its position (*Graham et al.*, 2012).

While there is strong observational evidence that the Southern Ocean is in fact warming throughout the water column (e.g., *Gille et al.*, 2001; *Böning et al.*, 2008) these same analyses suggest the change in transport is not significant. Nor is there any evidence in an increase in eddy kinetic energy derived from satellite altimeter sea surface height between 1993 and 2002 (*Meredith and Hogg*, 2006). Thus, there is significant work to be done to quantify and understand transport variability of the ACC. Here, we will utilize ocean bottom pressure gradients from satellite gravity to do this.

1.1.1 Calculating Transport Variability

Ideally transport variability along the ACC would be calculated by integrating the depth-integrated geostrophic current anomalies (Equation 1.1),

$$\Delta T(x,t) = \int_{y_\mathrm{s}}^{y_\mathrm{n}} \int_{-H}^{0} \Delta u(x,y,z,t) dz dy, \tag{1.1}$$

where Δ indicates an anomaly relative to the long term mean, u is the zonal geostrophic current, z is depth, t is time, x is the zonal direction (+ east), y is meridional direction (+ north), and y_n and y_s represent the northern and southern boundaries respectively. This calculation would give us the zonal transport across a section; the meridional component equation would be similar. However, since a majority of the ACC is zonal, our calculations will focus only on the zonal component.

A significant fraction of the variability in the ACC transport is associated with ocean bottom pressure (OBP) gradients across the fronts, from geostrophic balance

(e.g., *Nowlin and Klinck*, 1986; *Hughes et al.*, 1999). If one could measure OBP along a transect across the ACC, then the variability of the depth-averaged transport could be computed by integrating the gradient of ocean bottom pressure from south to north (*Hughes et al.*, 1999). Anomalies in depth-integrated geostrophic transport ($\Delta\bar{T}$) at any particular longitude (x) can be computed from the integral of the meridional gradient in OBP anomalies (ΔP) as,

$$\Delta\bar{T}(x,t) = \int_{y_\mathrm{s}}^{y_\mathrm{n}} \int_{-H}^{0} -\frac{1}{f(y)\rho(x,y,z)} \frac{\partial \Delta P(x,y,t)}{\partial y} dz dy = \int_{y_\mathrm{s}}^{y_\mathrm{n}} \int_{-H}^{0} \Delta\bar{u}(x,y,t) dz dy, \tag{1.2}$$

where f is the Coriolis parameter, ρ is the density of seawater, and H is the depth of the ocean, ΔP is in units of N/m^2, and $\Delta\bar{u}$ represents the depth-integrated geostrophic current anomaly.

Due to the lack of OBP data along transects *Hughes et al.* (1999) made several simplifying approximations to reduce Equation 1.2 to

$$\Delta T \sim -\frac{\bar{H}}{\bar{f}\rho}(\Delta P(y_\mathrm{n}) - \Delta P(y_\mathrm{s})), \tag{1.3}$$

where $\bar{H}$ is average depth made along a pseudo transect, $\bar{f}$ is average Coriolis parameter between y_n and y_s, ΔP is the bottom pressure anomaly north(n) and south(s) of the current, and ρ is mean density.

However, even having a pressure gauge north and south is uncommon. *Hughes et al.* (1999) also demonstrated using a model that the OBP south of the ACC was much larger than that north of the current, due to the much smaller area caused by the boundary imposed by Antarctica. They also showed a highly correlated OBP mode south of the ACC, which they called the "Southern Mode." *Hughes et al.* (1999) therefore suggested that a simple scaling parameter could be used to calculate trans-

port at the Drake Passage based solely on the OBP variations south of the current,

$$\Delta T_{\text{zonal}}(x,t) \sim \gamma \Delta P(y_{\text{s}}) \tag{1.4}$$

The scaling parameter (γ) would be determined from OBP variations and transport at the Drake Passage, both measured by the same model. This would allow for calculation of transport at the Drake Passage from just one bottom pressure recorder anywhere south of the SACCF or along the coastline of Antarctica.

When using the approximation calculation (Equation 1.3) it is assumed that the value of *H/f* does not vary significantly. However, in areas other than the Drake Passage, this is not necessarily the case due to submarine ridges located south of Australia in the Indian and Pacific Oceans that affect H and the broader scale of the fronts (Figure 1.1) which affects *f*. The typical scaling parameter used for Equation 1.4 is approximately -3 Sv/mbar of pressure south of the current (e.g *Hughes et al.*, 1999; *Zlotnicki et al.*, 2007; *Bergmann and Dobslaw*, 2012). *Hughes et al.* (1999) showed a high correlation of ∼-0.6, between BP south of the SACCF and transport in the model, but some areas had correlations significantly less than this. This suggests some potential complications with using a scaling parameter (Equation 1.4) or even an approximation approach (Equation 1.3) anywhere other than the Drake Passage. Figure 1.2 shows the percent variance of the transport as explained by OBP using data from the JPL_ECCO model (ecco.jpl.nasas.gov; Chapter 2.1.1) using Equation 1.4, compared to the full transport computed using Equation 1.1. The scaling parameter was determined by calculating the regression coefficient with respect to the transport through the Drake Passage measured using currents in the model. The recovered regression coefficient was similar to previous estimates (∼-3 Sv/mbar). At locations south of the current at the Drake Passage more than 75% of the transport variability is explained using OBP south of the current (Figure 1.2). However, at most other

longitudes, the variance explained is less than 60% and sometimes less than 50%. This emphasizes the problem of using the simplified equations (Equation 1.3 and Equation 1.4), except perhaps at the Drake Passage.

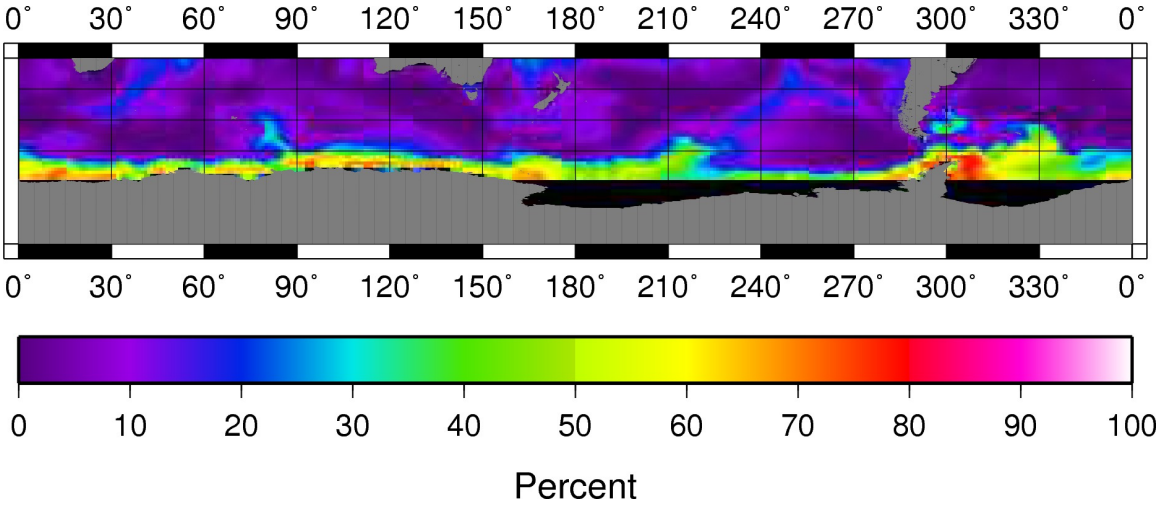

Figure 1.2: Map of the percent variance of transport through the Drake Passage as explained by ocean bottom pressure.

Along with issues arising from the approximation calculations, there are also issues with *in situ* measurements from bottom pressure recorders (BPRs). All BPRs drift, often by quite a bit. This will introduce low-frequency error into the signal. This type of instrumentation is also difficult to use for long time series, due to their limited life span and need for maintenance, which, although feasible in the Drake Passage, is not practical in other areas of the ACC. Figure 1.3 shows raw BPR data from three deployments made in the Drake Passage between 1998-2001 by the British Antarctic Survey. The data have not had drifts estimated and removed. Note that three separate BPRs were placed on the same deployment in 1998 and each had quite different drifts, some non-linear.

Models also tend to drift. Figure 1.4 shows the time series for transport anomalies through the Drake Passage from two different model simulations, one from the German Research Centre for Geosciences (GFZ) Ocean Model for Circulation and Tides (OMCT) and another the Jet Propulsion Lab's ECCO model, along with *in*

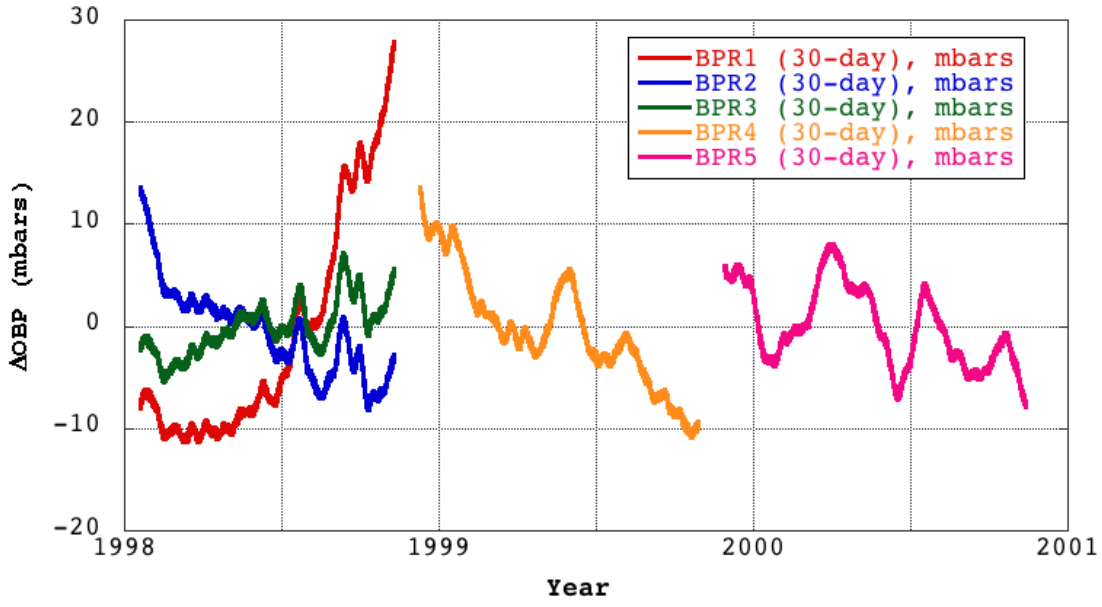

Figure 1.3: Time series of bottom pressure recorder data in Drake Passage. Archived at the British Oceanographic Data Centre (http://www.bodc.ac.uk)

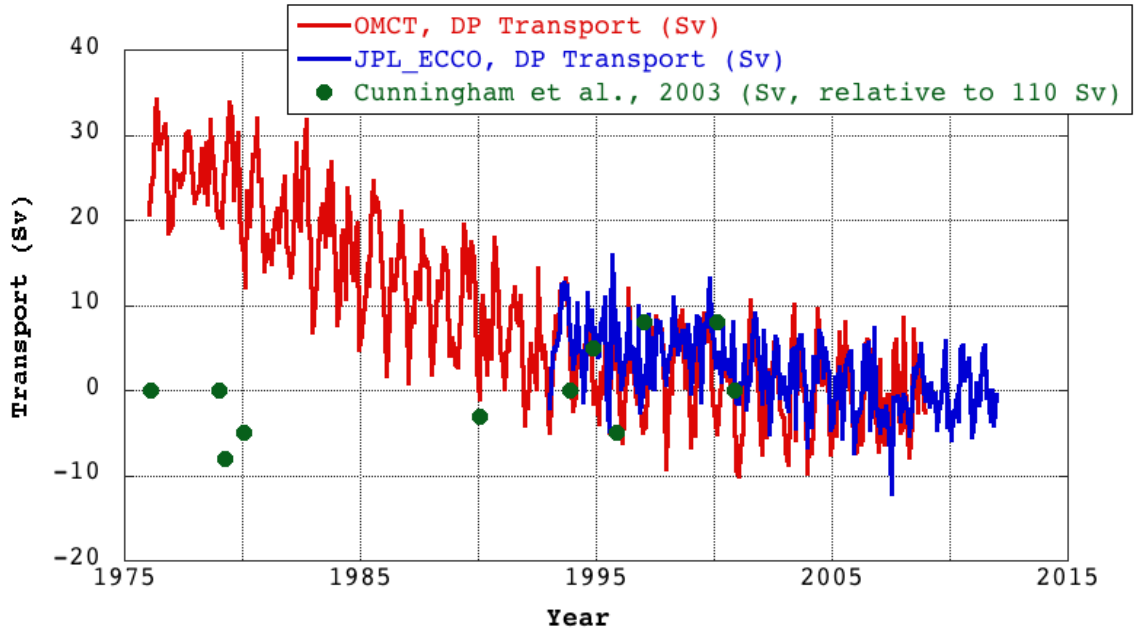

Figure 1.4: Time series of model data and in situ data. Note transport anomalies relative to a mean.

situ measurements from *Cunningham et al.* (2003) in the Drake Passage. The model transport was computed by scaling BP south of the SACCF by -3 Sv/mbar. The drift is most apparent in the OMCT model where the model is still adjusting state parameters at depth that likely had poor initial conditions at the beginning. Even the JPL_ECCO model, which assimilates data, indicates a statistically significant negative transport trend which is unlikely to be real and is probaly related to model drift.

1.2 The Gravity Recovery and Climate Experiment (GRACE)

The advancement of satellite technology now affords the use of innovative systems to look at long-term changes in many of the ocean's physical parameters (e.g., currents, sea level, ocean bottom pressure). The Gravity Recovery and Climate Experiment (GRACE) is one such system that will allow us to observe the low-frequency variability in the ACC transport via ocean bottom pressure. GRACE determines variations in gravity and mass indirectly, by measuring changes in range and range-rate between the two spacecrafts that comprise the GRACE satellite system (*Tapley et al.*, 2004). Other tracking data are combined along with accelerometer data to estimate gravitational coefficients in a least-squares state estimation problem to minimize the difference between the observations and a modeled orbit (*Bettadpur*, 2007). The gravity field potential is typically expressed as a finite spherical harmonic series (*Chambers and Schröter*, 2011),

$$V(R,\phi,\lambda,t) = \frac{\mu}{R} + \frac{\mu}{R}\sum_{l=1}^{N}(\frac{a_{\mathrm{E}}}{R})^{l}\sum_{m=0}^{l}P_{lm}(\sin\phi)\{C_{lm}(t)\cos m\lambda + S_{lm}(t)\sin m\lambda\}, \quad (1.5)$$

where V is the Earth's gravity potential, μ is the Earth's gravitational constant, a_E is the mean equatorial radius, R is the geocentric radius to the point, ϕ is the geocentric latitude, l is longitude, $P_{lm}(\sin\phi)$ are the fully-normalized Associated Legendre Polynomials of degree l and order m, and C_{lm} and S_{lm} are the fully-normalized spherical harmonic geopotential coefficients provided by the GRACE project. The gravity coefficients are computed approximately every month to degree/order 60, corresponding to wavelengths ∼666km at the equator.

Time-varying, non-tidal gravity coefficients $(\Delta C_{\rm lm}, \Delta S_{\rm lm})$ are computed by removing the time-mean and a model of tides. It is assumed that for periods less than several hundred years, the main cause of temporal changes in the gravity field is due to movement of water mass within the Earth's thin fluid envelope (*Wahr et al.*, 1998) so that the gravity can be converted to equivalent mass by

$$\Delta\sigma(\phi,\lambda,t) = \frac{a_{\rm E}\rho_{\rm E}}{3}\sum_{l=1}^{N}\sum_{m=0}^{l}\frac{2l+1}{1+k_{\rm l}}P_{lm}\{\Delta C_{lm}(t)\cos m\lambda + \Delta S_{lm}(t)\sin m\lambda\}, \qquad (1.6)$$

where $\Delta\sigma$ is the surface mass density in kg/m^2, $\rho_{\rm E}$ is the average density of the Earth (5517 kg/m^3), and $k_{\rm l}$ are Love numbers of degree l. Anomalies of ocean bottom pressure in terms of equivalent surface elevation are converted from surface mass density values by dividing by a mean ocean density of ∼1027 kg/m^3, or into pressure by multiplying by the acceleration due to gravity. To reduce the effect of error at an increasing degree, a Gaussian smoothing is also used (*Wahr et al.*, 1998).

Gradients in ocean bottom pressure anomalies are proportional to the depth average transport (Equation 1.2). It is important to note that although the literature has often indicated GRACE is only capable of measuring "barotropic" transport variations, this is used in the sense of changes in the depth integrated transport. GRACE is unable to distinguish whether the changes in depth averaged transport are due to a baroclinic or barotropic process. Thus, any change in the transport

that causes a depth integrated current fluctuation will have to be balanced by a pressure gradient change that is theoretically observable by GRACE. Due to the nature of the GRACE orbit and measurement, the gravity signals associate with zonal transport variability are better observed (with less error) than the meridional transport variability. A majority of the ACC transport is zonal and this study will focus on these areas where the circumpolar current is primarily dominated by the zonal component. Figure 1.5 maps the percent of transport variability described by the zonal component. This was calculated from currents in the ECCO model, integrated vertically and meridionally to get the transport (Equation 1.1). The total depth integrated transport variability is then calculated as

$$\Delta T(x, y, z, t) = \sqrt{\Delta T_{\mathrm{u}}^2 + \Delta T_{\mathrm{v}}^2}, \tag{1.7}$$

where ΔT_{u} is the depth integrated zonal transport anomaly and ΔT_{v} is the depth integrated meridional transport. The zonal transport variability was then divided by the total transport variability and multiplied by 100 to determine the percent of total transport variability that is explained by the zonal transport variability component. One can see that except in a few regions, notably south of New Zealand, the transport is more than 90% zonal.

Zlotnicki et al. (2007) were the first to use the earliest release of GRACE data to look at the zonal transport variability of the ACC using Equation 1.3. They averaged OBP from GRACE along the STF to the north and the SACCF to the south for three broad regions (Atlantic, Indian, and Pacific Ocean) and demonstrated that the GRACE data did correlate well with that from a model (e.g., 0.89 in the Pacific Ocean). However, the coherency was dominated by the seasonal cycle. They pointed to differences associated with leakage from melting of the West Antarctic ice sheet and noise from the GRACE data. They found a scaling between OBP south of the ACC and transport of $\sim$ -3 Sv/mbar, comparable to other studies with

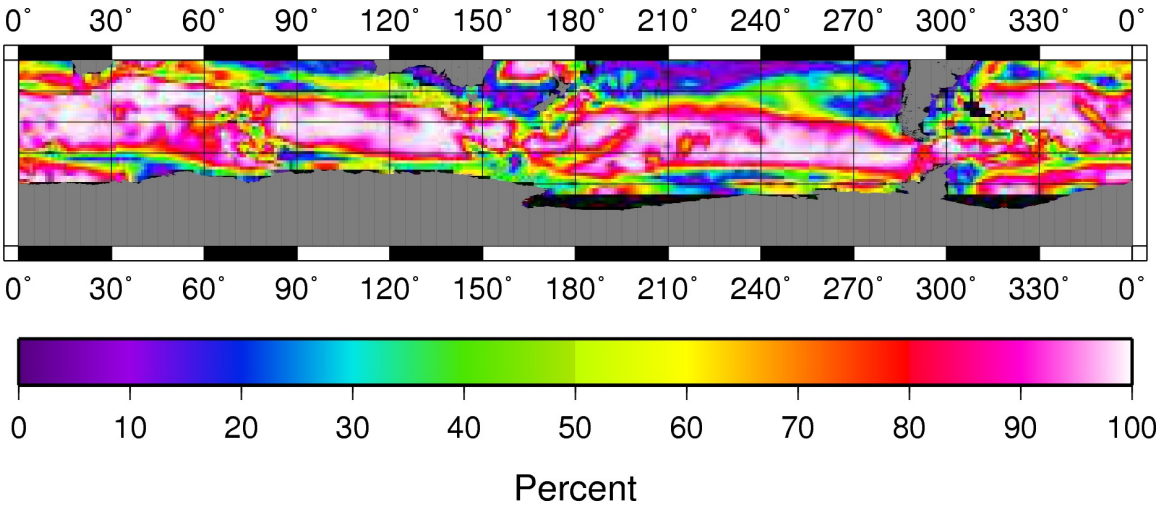

Figure 1.5: Map of the percent transport of the ACC as explained by zonal transport.

models. There were significant discrepancies with the amplitudes of the annual and semiannual cycles for GRACE and ECCO, however, which they suggested could have been either from errors in GRACE or the model being too sluggish in the ACC. The ECCO transport variations through the Drake Passage are noticeably smaller than those from the OMCT model in Figure 1.4.

Bergmann and Dobslaw (2012) used a more recent processing of GRACE data to look at higher frequency variability of the ACC at time-scales of less than a month. These products had previously been shown to be more accurate than models in the Southern Ocean at high frequency (*Bonin and Chambers*, 2011; *Ponte and Quinn*, 2009). *Bergmann and Dobslaw* (2012) also examined the correlation with the Southern Annular Mode (SAM) atmospheric index. They observed a correlation of 0.7 between the SAM index and GRACE derived transport. They found little correlation (0.3) between the SAM index and transport high-pass filtered to keep only periods less than 10-days. Their study found that transport calculated using GRACE OBP data is highly correlated with the Southern Annular Mode, which had been previously noted in studies using ocean bottom pressure recorders (*Hughes et al.*, 1999). Moreover, they demonstrated that GRACE is able to see consistent OBP patterns not seen by tide gauges along Antarctica which can be biased by local weather or ice effects,

and poor steric corrections (*Bergmann and Dobslaw*, 2012). Although they were able to increase the temporal resolution to observe the high-frequency transport fluctuations in GRACE, they still used larger basin averages similar to the *Zlotnicki et al.* (2007) study and also used the approximation equation (Equation 1.3). Additionally, they focused entirely on seasonal and shorter periods.

1.3 Research Project Summary

Ideally, we would like to have regular *in situ* observations of temperature, salinity, and currents at all depths at regular temporal and spatial intervals across the Southern Ocean to create a complete time series of the transport variability of the Antarctic Circumpolar Current. This would improve our understanding of climatic changes in the transport and increase the skill of transport predictions. However, due to the limitations of *in situ* instrumentation and errors associated with the ocean models discussed in Section 1.1, we are limited to few options for creating a time series of the transport variability to observe low-frequency changes. GRACE OBP data, therefore, provides a unique data set to study transport variability of the ACC.

This research will focus on low-frequency, zonal transport variability of the ACC, especially trends and interannual variability in transport fluctuations, and examine correlation between transport variability and local, regional, and large-scale wind forcing, including the Southern Annular Mode (SAM) index. Ocean bottom pressure data from GRACE has previously been used in large basin-wide averages (Section 1.2), and utilized an approximation to derive transport. There are four main issues to address from previous studies. The first issue is the approximation technique, which was derived for narrow latitude bands of the Drake Passage where H and f do not vary considerably (Equation 1.3). The next issue to address is that ocean bottom pressure was used along the STF in the Pacific, which is a weakly defined front and

does not form a strong northern boundary of the ACC in this region. Another issue from previous studies was that most transport calculations were averaged over large longitudinal averaging areas and included data near the West Antarctic ice sheet, which is known to contribute leakage to the GRACE signal (*Zlotnicki et al.*, 2007). Finally, many investigations based their uncertainty analysis by comparing to ocean models which are known to have comparable errors in OBP in the Southern Ocean to GRACE (e.g., *Chambers and Bonin*, 2012).

This research aims to address the above mentioned issues. We will use the full integral equation (Equation 1.2), instead of the approximation (Equation 1.3), and will include the variability of H/f. In order to better quantify the uncertainty of the GRACE data, we will use multiple realizations of a simulated data set with realistic GRACE-like errors instead of comparing to a single ocean model run. A minimal spatial averaging will be used to quantify transport variations, as opposed to large, almost basin-scale averaging distances. Finally we will focus primarily on the low-frequency transport variations, which have previously not been studied due to the drift in BPRs and a preconception that GRACE can only detect variations that have periods shorter than 1-year.

The research area will be focused away from the Drake Passage (an area already extensively studied) and the West Antarctic ice sheet, to avoid the addition of error from leakage of ice sheet melting. Previous studies have focused on the Drake Passage choke point, mainly because it is relatively easy to reach and instrument due to its narrowness. The spatial resolution of GRACE and leakage from the West Antarctic ice sheet increase the uncertainty in trends when calculating transport at this location. The African choke point also is a challenge when using GRACE data, due to the strong, narrow return flow of the Aghulas current. The transect near 140°E bounded by Antarctica to the south and Tasmania to the north, however, is another commonly examined choke point (*Rintoul and Sokolov*, 2001). A choke point calculation at this

location will prevent the addition of potential error associated with using the Sub-Tropical Front position as a northern boundary, since the front positions have been observed to be a strong boundary of the ACC there. This is also an area where a majority of the transport variability is described by the zonal component (Figure 1.5). Due to the limitations of transport calculations from GRACE at the Drake Passage and African choke points and the more ideal conditions of the Tasmania-Antarctica choke point, this research focuses on the longitudes between 120°E and 160°E.

We begin by determining the uncertainty of transport calculations using GRACE OBP. We have quantified these uncertainties using a simulated data set described in Section 2.1.2 and the JPL_ECCO ocean model. Chapter 2 covers the statistical tests used to quantify this uncertainty, and the results of these statistical analyses.

Having quantified the uncertainty in transport calculations from GRACE, we then approach the main scientific questions of this project in Chapter 3. We first quantify the low-frequency zonal transport variability around 140°E longitude transect line and assess whether there is any statisticaly significant trend. We then investigate the mechanisms by which local winds force low-frequency variability and the effect the average Southern Hemisphere winds have on transport variability at the Tasmania-Antarctica choke point.

Chapter 2

Assessing Uncertainty of Transport Computed from GRACE

In order to quantify the uncertainty and errors associated with transport calculations using GRACE ocean bottom pressure data, a statistical analysis was conducted based on output from an ocean model run at the Jet Propulsion Laboratory (JPL) as a contribution to the Estimating the Circulation and Climate of the Ocean (ECCO, www.eccogroup.com) and a simulated set of gravity coefficients that include hydrology, ocean, and cryosphere signals as well as GRACE-like errors. The uncertainty of trend estimates, seasonal amplitudes, and coherency between ECCO and the GRACE-like data will be discussed. Section 2.1 describes the data sets in more detail, while section 2.2 presents results of statistical tests.

Figure 2.1 maps the mean total transport for each 1° grid of the ACC, in the ECCO model we use along with the *Orsi et al.* (1995) front positions. The mean total transport for each 1°x1° grid was calculated from currents at depth in the ocean model, hereafter referred to as JPL_ECCO, using Equation 1.1. The *Orsi et al.* (1995) fronts do not necessarily match the core transport of the ACC (areas where transport variability is $\geq$9 Sv in the model), which suggests either dynamic front positions or deficiencies in the model. The disparity is largest from 0°-90°E, but in general the fronts bound the main transport in other regions, indicating the model is sufficient

for our testing.

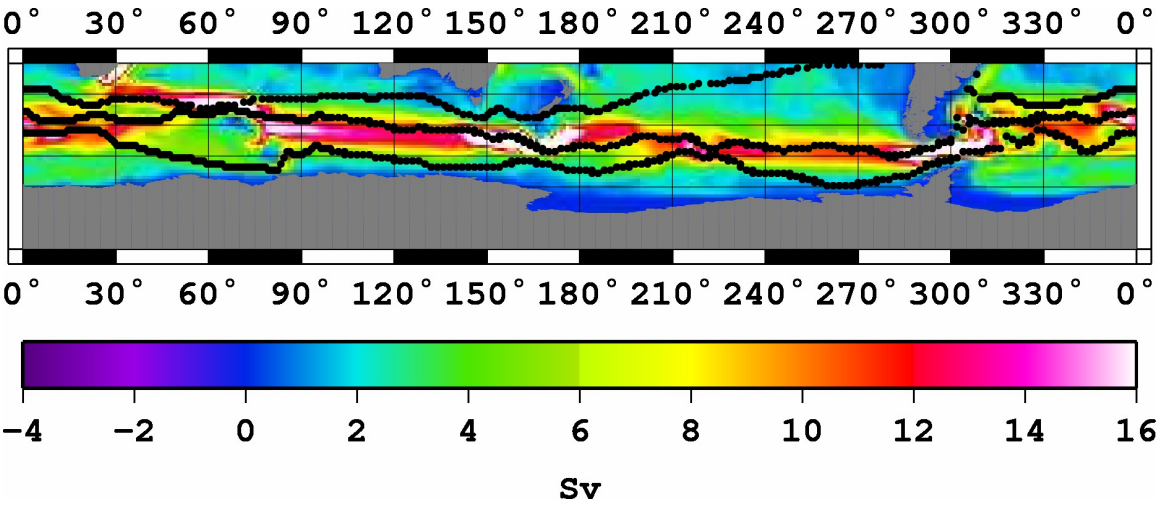

Figure 2.1: Map of mean total transport for each 1° grid from 2003-2010 calculated using JPL_ECCO currents at depth. In black are the front positions (from *Orsi et al.* (1995)).

2.1 Data Sets

2.1.1 Ocean Model

The JPL_ECCO ocean model is used as the "truth" ocean bottom pressure data for our analysis. The JPL_ECCO model is based on the MIT general circulation model and is run at the Jet Propulsion Lab (JPL) as part of the Estimating the Circulation and Climate of the Ocean (ECCO) consortium. It is a baroclinic model forced by winds, pressure, and heat and freshwater fluxes from the National Center for Environmental Prediction (NCEP) operational analyses products and also assimilates satellite altimetry and other *in situ* observations (*Fukumori*, 2002; *Kim et al.*, 2007). It is eddy parameterized with 1° x 1° resolution over the Southern Ocean. The model output is available as both 10-day averages of velocities at depth and monthly averages of ocean bottom pressure. The OBP is output as monthly averages to be consistent with the GRACE averaging period. We use the OBP data as the base for our simulated data

set, obtained from the Tellus website (http://grace.jpl.nasa.gov/data/ECCOOBP).

2.1.2 GRACE Simulated Data Set

The GRACE observations do have some significant problems, especially when using them to study ocean mass variations. One issue faced is a correlated error that causes north-south stripes in the mapped GRACE data (*Swenson and Wahr*, 2006). In order to use GRACE data over the ocean these problems must be corrected via post-processing. We use a method described in detail by *Chambers and Bonin* (2012). The first step involves "de-striping" the coefficients to remove a significant fraction of the correlated error and mapping over the ocean as described in Section 2.1. Another of these issues is that the signal from land hydrology fluctuations and mass losses from ice sheets, on the order of 50 times larger than ocean mass variations, and a significant amount of this signal will leak into the ocean around land. To reduce this, the original gravity coefficients are mapped at the highest resolution (60 x 60 spherical harmonics shown as a 1°x1° grid) with no de-striping or smoothing, the ocean grids are masked out, and the new maps are re-converted to spherical harmonics. These "land only" coefficients are then destriped and smoothed, then mapped over the ocean to estimate the leakage. This is subtracted from the first calculation to remove as much of the leakage as possible. Although, the leakage will not be completely removed, the corrected data do have a smaller error associated with leakage along the coastlines and interior ocean than if this is not done (Figure 2 in *Chambers and Bonin* (2012)), although higher residual errors remain around Greenland and West Antarctica. The latest Release-05 has improved the quality of GRACE data over the ocean, with standard errors of $\sim$1 cm of equivalent water thickness over most of the ocean (*Chambers and Bonin*, 2012).

Previous studies investigating transport from GRACE data have simply differenced results with those obtained from models (e.g., *Zlotnicki et al.*, 2007; *Bergmann*

and Dobslaw, 2012). This will tend to be too pessimistic, as models have comparable errors to GRACE in the Southern Ocean (*Chambers and Bonin*, 2012). Instead of this approach, we quantify the uncertainty in transport calculations using a large number of simulated data that mimic GRACE errors. The simulated GRACE gravity coefficients include land hydrology variability, glacial isostatic adjustment (GIA), mass loss from both Greenland and Antarctica, ocean bottom pressure variability, and a model of correlated and random GRACE errors (*Bonin and Chambers*, 2013). The OBP variability is that from our "truth" determined from JPL_ECCO. The important part of this calculation was the generation of correlated errors to create stripes in mapped data (Figure 2.3). Although spatially correlated, the stripes are random in time (*Bonin and Chambers*, 2013).

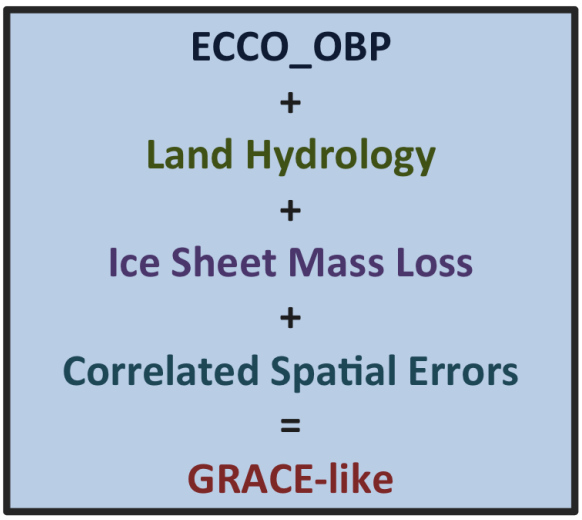

Figure 2.2: Flow chart of how GRACE-like simulation data set is developed.

Since the GRACE-like error model is initialized from a random starting kernel, we can produce numerous different realizations of the error to compute more robust statistics. We created 100 realizations that were processed into maps of OBP from which transport can be calculated. The simulated data were mapped using the method described by *Chambers and Bonin* (2012), which includes the same destriping, leakage correction, and smoothing with a 500km Gaussian filter.

Figure 2.3 shows maps of the GRACE-like OBP data along with those from actual GRACE RL05 data, at varying processing steps. Note that the simulated data should not be expected to be identical to the observations. We merely expect the level of errors and signal to be similar. Figure 2.3e&f compares the GRACE-like and GRACE RL05 data after destriping and applying a 500km Gaussian filter. Note the slightly larger signals in the ocean in the simulated data after processing (Figure 2.3f), which suggests the error model may be more pessimistic than the true GRACE-errors. Thus, our analysis is likely to overestimate, rather than underestimate uncertainty. Monthly OBP maps for each simulation were created for the period from January 2003 until December 2010.

2.1.3 Depth Data

We use bathymetry (H) from ETOP01 (*Amante and Eakins*, 2009), averaged to a 1° grid consistent with the model resolution and OBP maps.

2.2 Results and Analysis

In order to quantify the uncertainty bounds for the GRACE estimates of transport variability we compute statistics of the 100 realizations of the GRACE-like data described in Section 2.1.2. This allows for a more robust analysis, and also accounts for the potential range of spatial and temporal errors. The simulated GRACE data were observed to have a slightly higher variance (1.1 times higher standard deviation) than real GRACE data as discussed in Section 2.1.2. This was discovered after creating and post-processing all 100 realizations, which took two days of computation time. To reduce the time required to repeat the calculations, we simply scaled OBP in the simulation by 0.9 to account for the difference in variance.

We begin by calculating time-series of zonal transport variability using Equa-

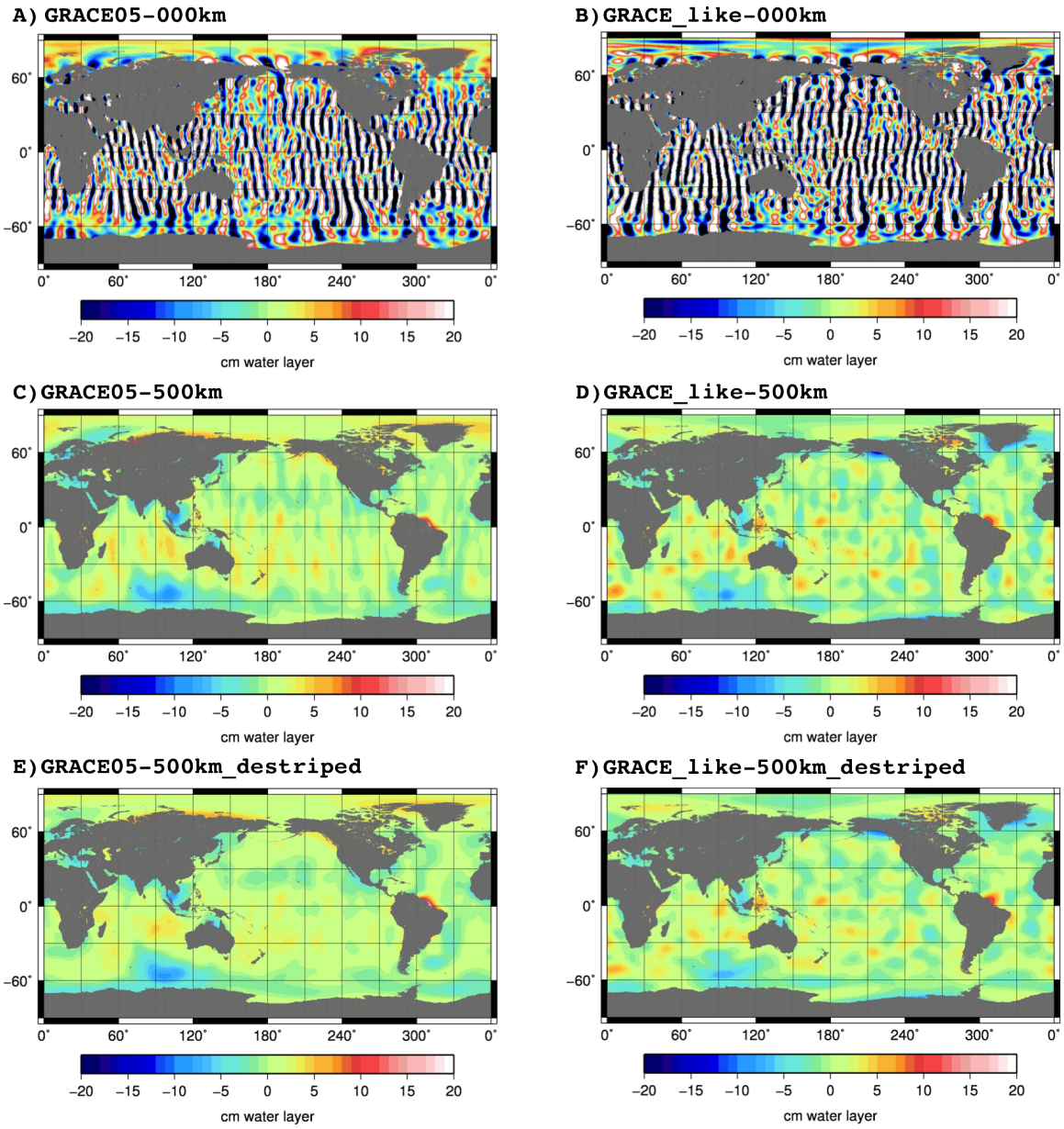

Figure 2.3: Comparison of GRACE and GRACE-simulated contour maps. a) 000km unsmoothed GRACE-simulated, b) 000km GRACE, c) 500km smoothed GRACE-simulated, d) 500km smoothed GRACE, e) 500km smoothed and destriped GRACE-simulated, f) 500km smoothed and destriped GRACE. All images have a land leakage masking procedure applied. Scale is in cm of equivalent water thickness.

tion 1.2 for a range of latitudes around the 140°E transect using both the simulated GRACE-like data after processing and the JPL_ECCO OBP data with no temporal or spatial smoothing. The latitude bounds used were the position of the Sub Tropical Front (according to the *Orsi et al.* (1995) front positions) and -62.5°S as the southern boundary. Since the JPL_ECCO OBP formed the ocean component of our simulation, differences represent errors from GRACE noise, residual leakage, and the de-striping and smoothing algorithm.

The transect time series were then averaged spatially in order to determine an optimal spatial averaging area that reduces the noise of the time-series with little decrease in the correlation. This is based on average standard deviation and correlation of the 100 realizations. Previous studies looked at average bottom pressures computed over much larger longitudinal areas (e.g., the entire Pacific), then differenced these (north-south) to determine the bottom pressure gradient (e.g., Equation 1.3). We calculated transport variability over multiple spatial averaging areas ranging from $\pm$ 2° to $\pm$30° from 140°E at 2° increments using the full integral equation (Equation 1.2). Figure 2.4 shows the zonal transport variability time series calculated from one realization of the GRACE-like data and JPL_ECCO along a single transect at 140°E. Overall, the GRACE-like transport (blue) agrees well with the ECCO (red), "truth", calculated transport except in some cases (June 2004, late 2006) where there are short-period excursions. These are likely differences between the ECCO model and GRACE-like in the high-frequency signals, possibly from the different parameterizations between the two data sets.

In Figure 2.5, the average standard deviation of the transport residuals for all 100 realizations is shown as a function of the spatial averaging area. Also shown is the mean standard deviation of JPL_ECCO transport over the same area. The model transport standard deviation is 5-5.5 Sv (Figure 2.5), and doesn't change much even when averaged over 60° of longitude. The residual standard deviation drops below 4

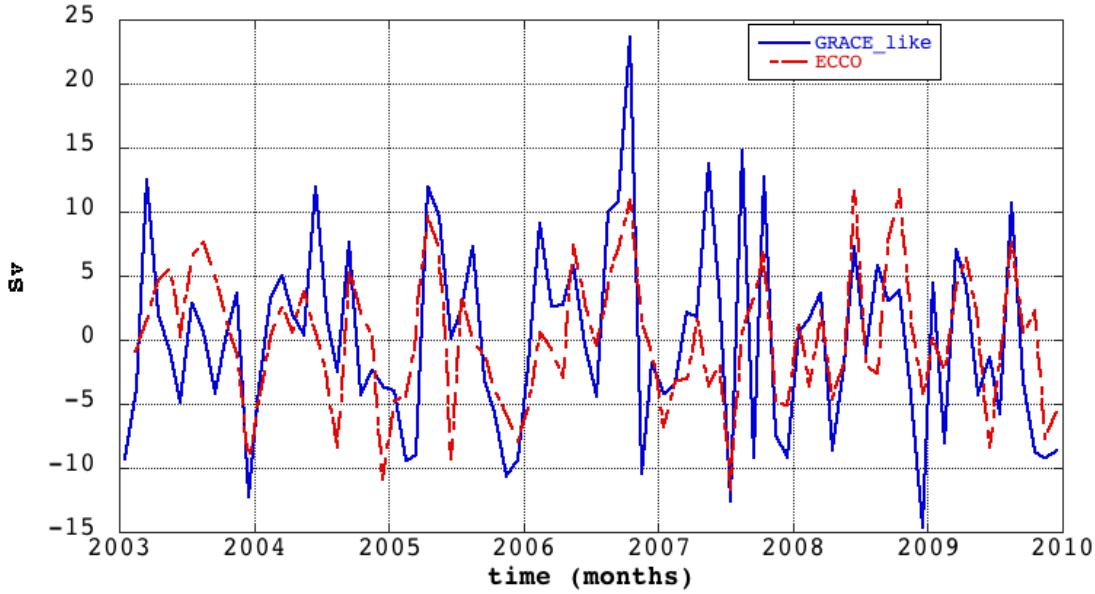

Figure 2.4: Time series of transport calculated from GRACE-like and JPL_ECCO data for a single transect 140°E.

.

Sv at an averaging area of ±15° (30° longitudinal averaging area), and does not change much more even to ±30° of averaging area. The average correlation between the 100 realizations and JPL_ECCO time series as a function of spatially averaging area is shown in Figure 2.6. The correlation goes above 0.7 as the ±15° spatial averaging area is approached and then changes only slightly at higher spatial averaging areas.

The amplitudes of the seasonal cycle and trends were calculated for the transport time series of each realization using a standard least squares estimation. We calculate the average root mean square (RMS) of the differences in ECCO-GRACE-like trends and seasonal amplitudes at the various different spatial averaging areas instead of calculating the mean standard deviation. This is done because there are small, consistent biases in the residuals which will be reflected in the RMS and not standard deviation. The biases are likely from uncorrected leakage, possibly from the northern boundary (Australia). The RMS of the seasonal amplitude differences for

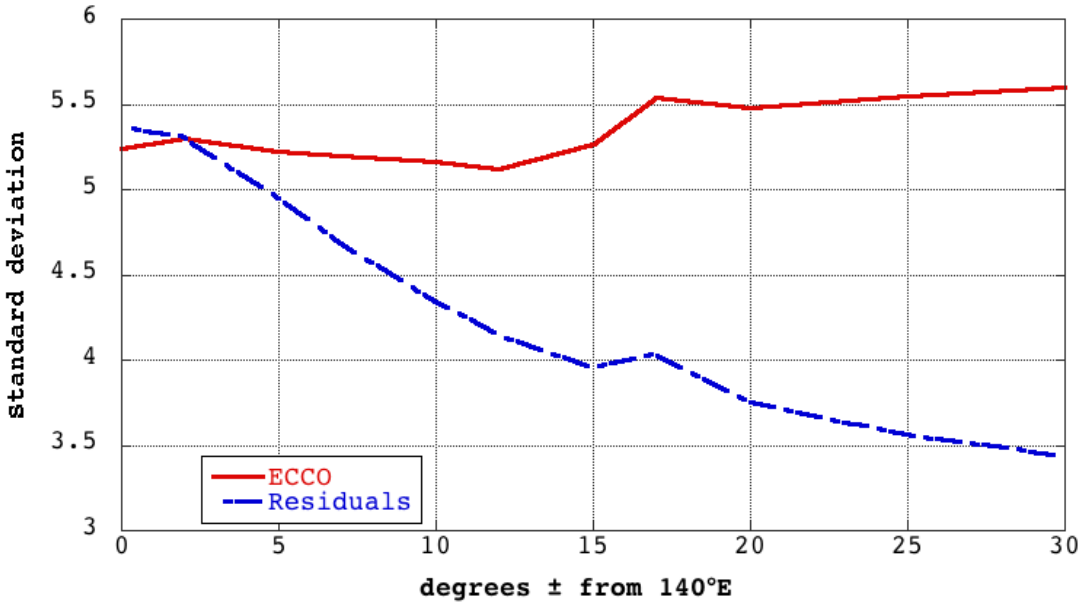

Figure 2.5: Mean standard deviation of ECCO and GRACE-like residuals relative to the ECCO signal compared to spatial average width. ECCO (red), GRACE-like (blue).

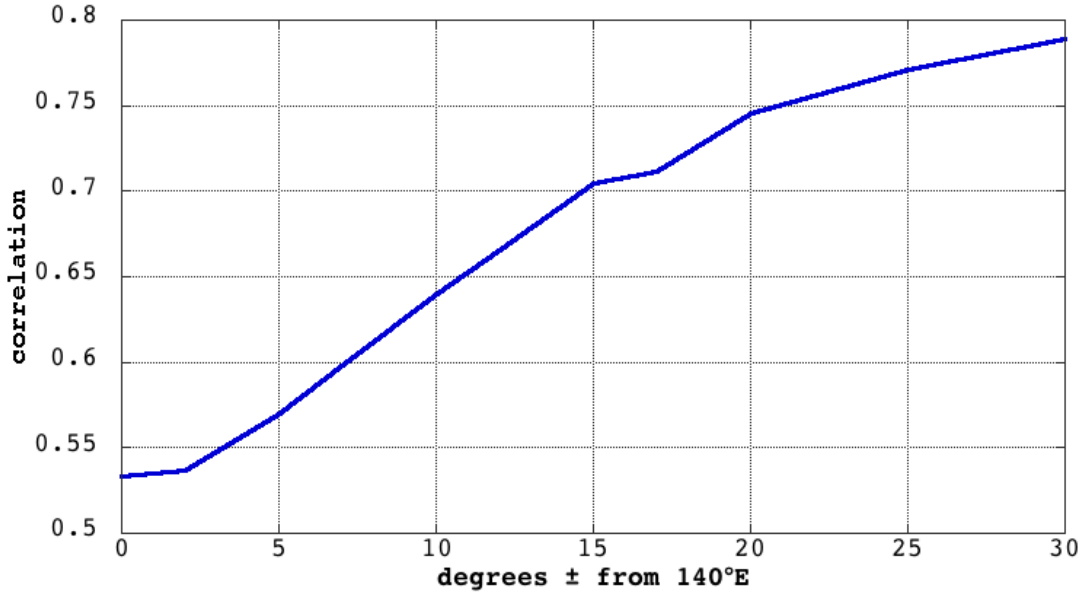

Figure 2.6: Mean correlation of GRACE-like and ECCO for each spatial averaging area.

each spatial average is shown in Figure 2.7. The RMS of the trend differences for each spatial average area are shown in Figure 2.8.

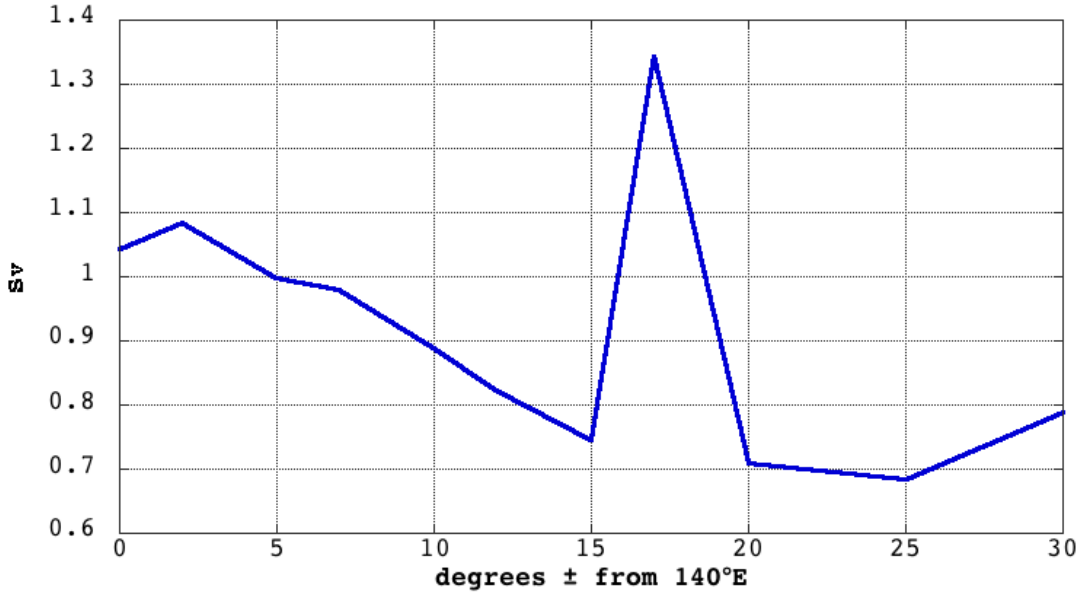

Figure 2.7: Root mean square of amplitudes from least squares estimation for each spatial averaging area.

The RMS of the seasonal amplitude and trend differences drops to a low of 0.75 Sv and 0.26 Sv/year at ±15° before jumping to higher values at ±17°. There is a noticeable "kink" at ±17° seen in the standard deviation and correlation statistics (Figures 2.5 & 2.6) and in the mean transport variability (Figure 2.5), where transports are about 0.5 Sv higher for larger averages suggesting some sort of change between the zonal transport between 125°E-155°E and that of the larger areas. This suggests a distinct change in transport east of 155°E or west of 125°E, possibly due to the constriction of fronts around 155°E(Figure 2.1). There is also the possibility of a bias in the mean of one of the transects averaged over the ±17° area that could be effecting the RMS of the amplitude and trend being calculated at this averaging area.

We next applied temporal smoothing to the time series at each transect be-

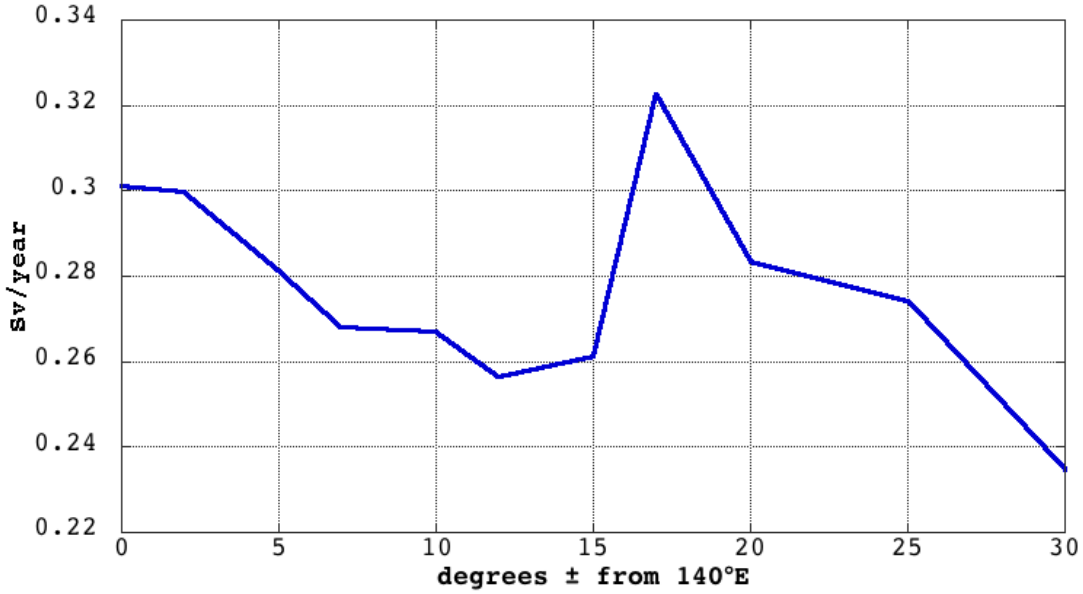

Figure 2.8: RMS of trends from least squares estimation for each spatial averaging area.

fore spatial averaging, using a low-pass filter based on a 2-month Gaussian weighted average, where the weights are calculated from

$$weights = e^{-0.5(\frac{dt}{2})^2}, \tag{2.1}$$

The filter was applied after first removing the seasonal signal from the GRACE-like and JPL_ECCO transport series, estimated using linear least squares, in order to better isolate uncertainty of the non-seasonal, low-frequency transport variability. The correlation decreased by approximately 0.05 between GRACE-like and ECCO after applying the low-pass filter which suggests that the previous, higher correlations were caused in part by the seasonal signal (Figure 2.9). However, the correlation is still high and significant at $\sim$0.67 for the $\pm 15^\circ$ average. The standard deviation dropped considerably after applying the low-pass filter, from $\sim$4 Sv to $\sim$1.5 Sv. This is similar to the change in variability of the "true" (JPL_ECCO) signal after the low-

pass filter is applied, again due to the removal of the large seasonal variations. Note that with no spatial smoothing, the low-pass filtered GRACE-like data have higher errors than the expected signal. However, the error is decreased significantly at larger averaging areas greater than $\pm 5°$.

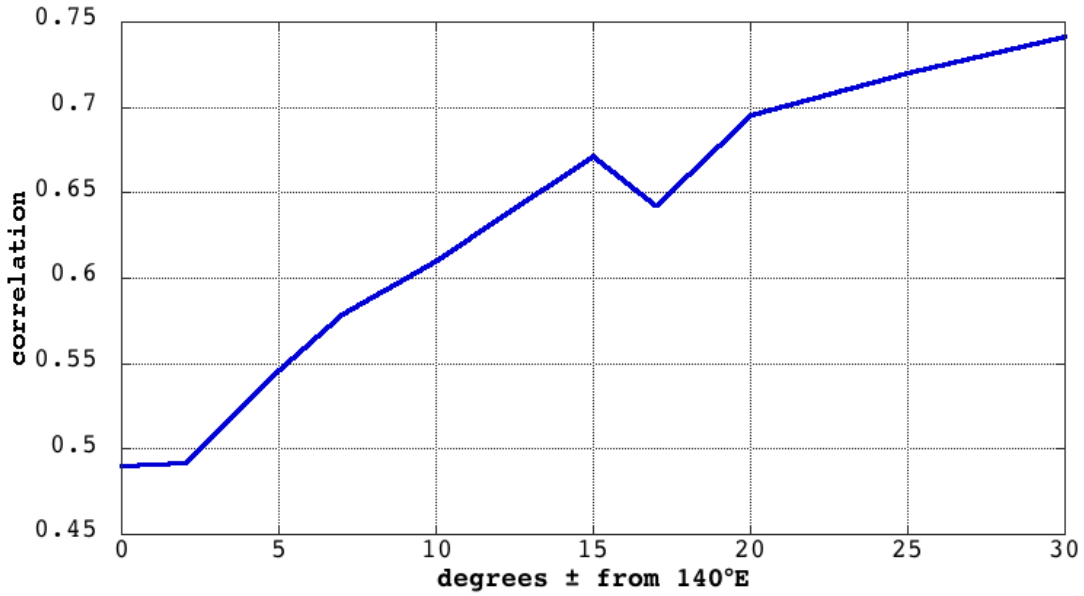

Figure 2.9: Mean correlation of GRACE-like and ECCO for each spatial averaging area, after temporal smoothing.

2.3 Conclusions from Statistical Testing of Simulation

The analysis described in Section 2.2 allows us to place error estimates on transport variability calculations made using GRACE OBP. By applying different degrees of spatial averaging, we have been able to determine an averaging area most appropriate and beneficial to reduce noise and maintain signal variance. Based on the decrease in the standard deviation, reduction in trend and seasonal amplitude differences, and increase in correlation between the two data sets, we will use an average

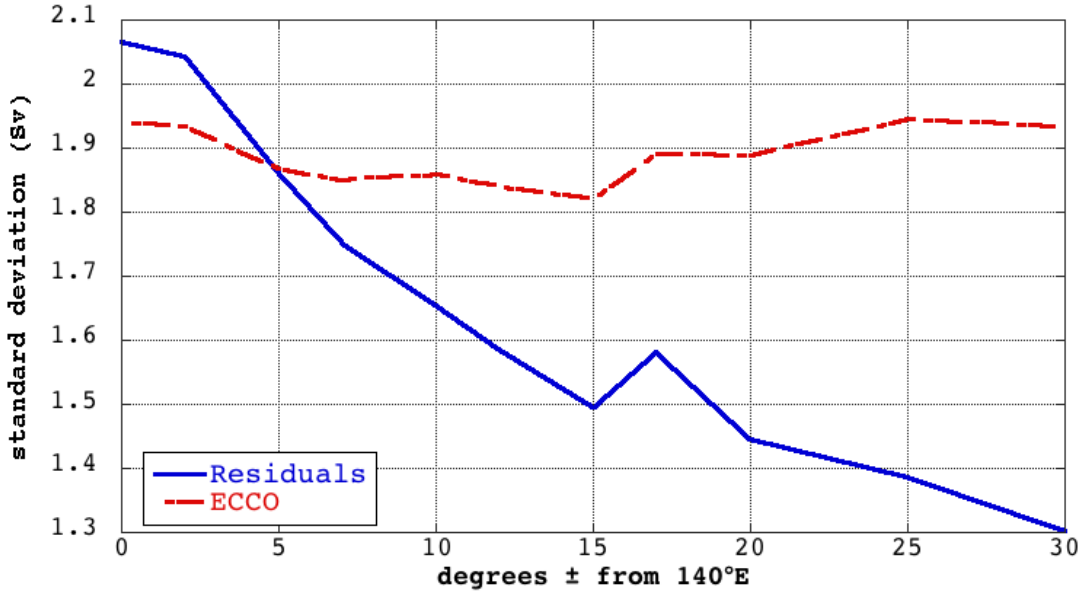

Figure 2.10: Mean standard deviation of GRACE-like - ECCO residuals for each spatial averaging area, after temporal smoothing.

area of 140°E ±15° longitude (125°-155°) for further analysis. Since there are no drastic improvements in spatially averaging more than ±15°, this study will focus on monthly transport variability calculated over this spatial averaging area. More spatially averaging does not significantly improve the statistics, and there is evidence of a change in behavior going beyond ±15°.

The results indicate that by spatially averaging over the 125°E-155°E area we significantly increase the signal-to-noise ratio for monthly and low-frequency signals. Residuals between the simulated and "truth" data are nearly random, with little autocorrelation at lag = 1 month. Based on the random residuals and RMS statistics of trend differences, this suggests that GRACE data can be used to observe a trend in the transport greater than ±0.4 Sv/year at 90% confidence with at least 7-years of observations.

Chapter 3

Evaluation of ACC Transport Variability and Southern Hemisphere Winds

The relationship between low-frequency transport variability of the ACC and Southern Hemisphere (SH) winds is still an area largely understudied. Even in areas of high sampling frequency, such as the Drake Passage, there are still few previous studies that have focused on the low-frequency variability in transport and the relationship with winds (Chapter 1). Based on the results of the statistical analysis discussed in Chapter 2, we will use GRACE OBP data as an observational data set to quantify the relationship winds and the transport variability of the ACC at the Australia-Antarctica choke point at low-frequencies.

3.1 Transport Variability from GRACE OBP Data

Figure 3.1 shows the time series of the zonal transport variability averaged over 125°E-155°E (Australia-Antarctica choke point) calculated using both GRACE OBP and ECCO OBP data. The error bars for the GRACE measurements are calculated based on the results from the error analysis discussed in Chapter 2, specifically Section 2.2. Although, the ECCO model has similar variability in transport as GRACE, there are several periods where the two estimates differ by more than the estimated error.

Specifically, for some months in 2003, 2004, and late 2005, GRACE estimates a larger transport than ECCO while in 2009 GRACE estimated transport is lower. These differences are all outside the error bounds estimated for GRACE, and may reflect deficiencies in the model. Even with these differences, the two time-series do have a high correlation (0.68, significant at the 90% confidence level). Both transport time series show a similar annual signal, with transport higher in the middle of the year.

The trend and the amplitude of the seasonal cycle observed from the GRACE OBP data were calculated using linear least squares estimation. The trend observed from the GRACE OBP is -0.3±0.4 Sv/year (90% confidence from analysis in Section 2.2), which is not significantly different from zero, suggesting no long-term suggest an increase or decrease in the transport of the ACC at the Australia-Antarctica choke point. The seasonal amplitude is 5.1±1.5 Sv (90% confidence level). There is a slight positive trend in ECCO-derived transport of 0.2 Sv/year and the seasonal amplitude is 2.4 Sv. The seasonal amplitude of GRACE is about twice that of the ECCO estimated seasonal amplitude, but closer than found in previous studies. *Zlotnicki et al.* (2007) found that the seasonal amplitude using an earlier release of GRACE was 11 Sv and an older version of ECCO was 4 Sv. The results from this analysis do bring down the GRACE seasonal amplitude to what the older version of ECCO produced, however the ECCO amplitude was also reduced. These differences could be attributed to the larger averaging area that *Zlotnicki et al.* (2007) used. Thus, neither transport estimate suggests a change in the ACC transport and both agree within the uncertainty.

A low-pass filter was applied to the transport variability time-series after removing the estimated seasonal signal to better isolate the low-frequency, non-seasonal signal in the transport variability. The filter is the same low-pass, Gaussian filter used in the error analysis calculations (Equation 2.1) with a 2-month roll off. The time series for the transport variability calculated using both GRACE OBP and ECCO

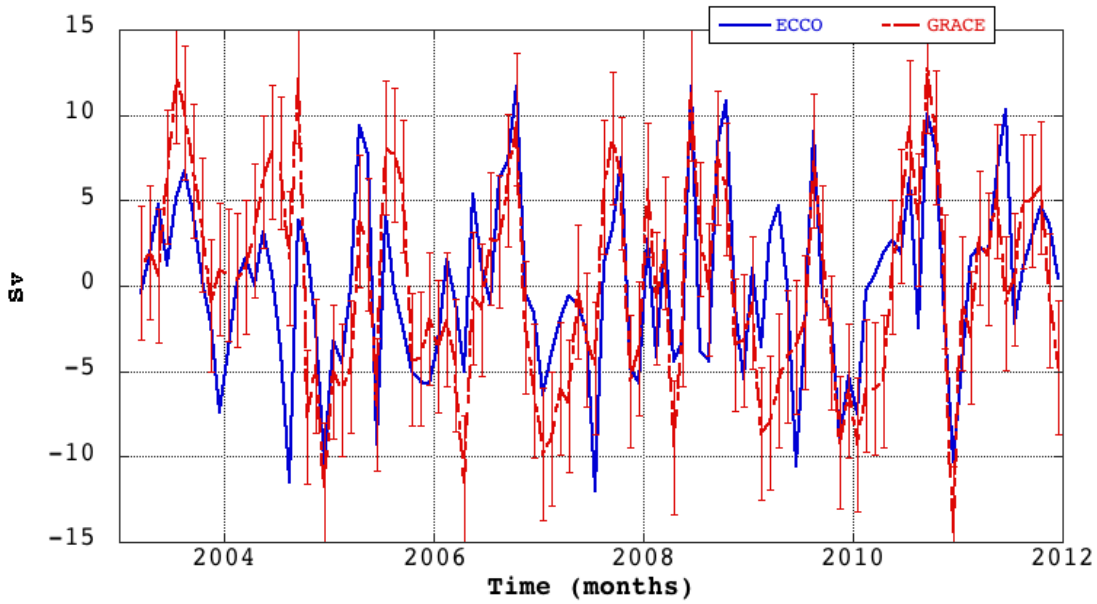

Figure 3.1: Time series of transport variability averaged between 125°E-155°E using GRACE OBP (red) and ECCO OBP (blue). Error bars are calculated based on results from Section 2.2.

OBP are shown in Figure 3.2. There are several periods where there are significant difference between the GRACE and ECCO estimations, notably GRACE observes a higher transport than ECCO in 2003-2004 and the end of 2007, the beginning of 2008, and a lower transport in 2006/2007 and in late 2009. Again, we attribute these differences to potential errors in ECCO as they fall outside our estimated uncertainties for GRACE. At the low-frequency the correlation between GRACE and ECCO, while significant at 90% confidence, is low at 0.46. This is much lower than the unfiltered time-series previously discussed. The drop in correlation is partly due to the removal of the seasonal period, but also due to the different trends. When the trends are removed from both of the time-series, the correlation increases slightly to 0.50.

While there are similar variations in transport shown in both GRACE and ECCO, there are still some significant differences which we again attribute to deficiencies in the model, based on our error analysis from Chapter 2. The residuals

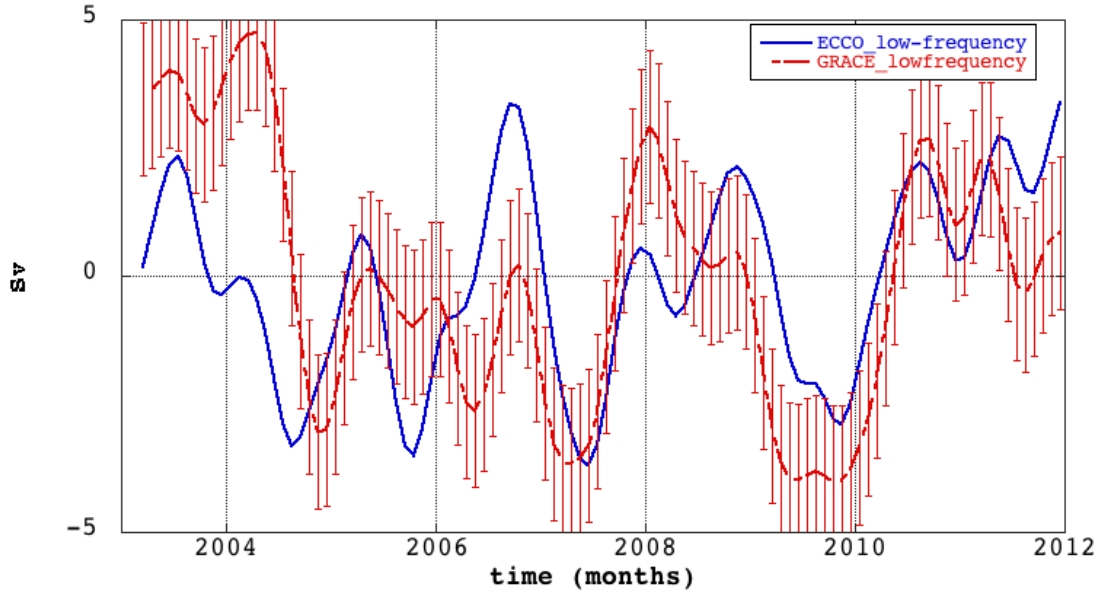

Figure 3.2: Time series of low-frequency transport variability averaged between 125°E-155°E using GRACE OBP (red) and ECCO OBP (blue).

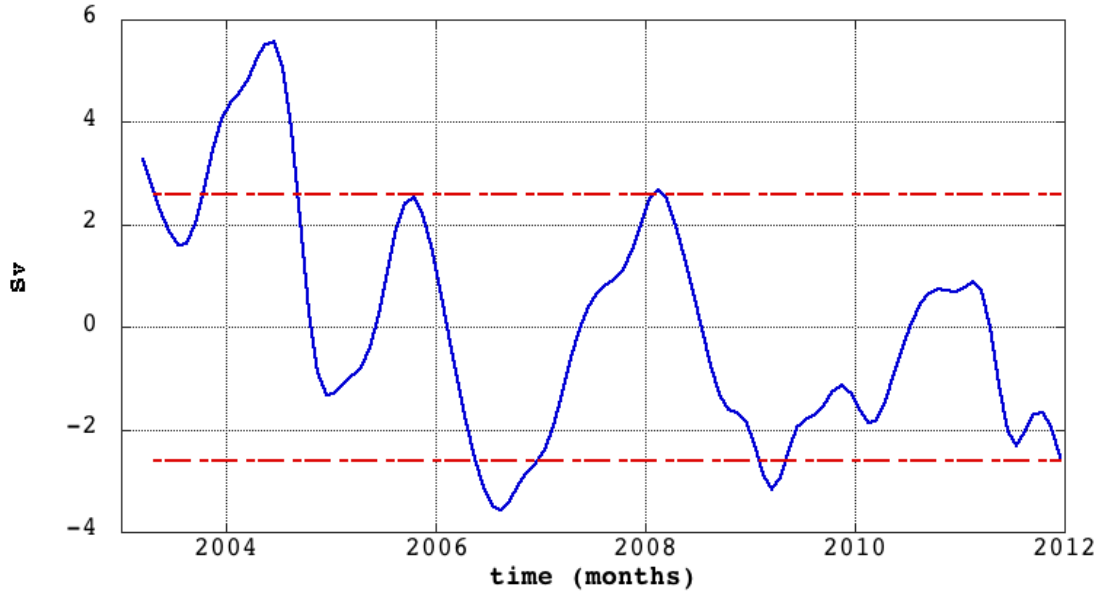

Figure 3.3: Time series of low-frequency transport variability averaged between 125°E-155°E using GRACE OBP (red) and ECCO OBP (blue) compared to residuals (green) between GRACE and ECCO calculated transport.

between GRACE and ECCO calculated transport variability are plotted along with the monthly error estimates from GRACE at the 90% confidence level (±2.6Sv) in Figure 3.3. There are areas where the residuals fall outside of the error bounds, suggesting that the differences between the transport variability calculated from the model and observations in these areas are related to model error.

3.2 Comparison of Transport Variability and the Southern Annular Mode (SAM)

The Southern Annular Mode (SAM), also known as the Antarctic Oscillation (AAO), is the leading mode of atmospheric variability in the Southern Hemisphere in many atmospheric fields including zonal wind and surface pressure (*Marshall*, 2003). It is dominated by an alternation of atmospheric mass over Antarctica and the Southern Ocean, impacting both the location and magnitude of the zonal winds in the Southern Hemisphere (*Lovenduski*, 2005).

The variability of the SAM is often represented as a normalized SAM (or AAO) index and this is often used to represent the variability of SH winds. Two commonly used SAM indices (low-pass filtered) are shown in Figure 3.4. The first is from the University of Washington's Joint Institute for the Study of the Atmosphere and Ocean (JISAO) based on anomalies at the 850-hPa geopotential height obtained from a spectrometer and the National Center of Environmental Prediction (NCEP) model (http://jisao.washington.edu/aao/slp/; *Thompson and Wallace* (2000)). This index use Principal Component Analysis to determine the leading mode of variability and uses this as the index. Finally, the index of *Marshall* (2003), from the Natural Environment Research Council (NERC) British Antarctic Survey, is based on sea level pressure (SLP) from 12 different stations in the Southern Ocean. The SLP 6 stations from the higher latitude band (∼70°S) and the 6 stations from lower latitude

(∼40°S) band of the SAM index are averaged and then differenced between the two latitude bands (http://www.nerc-bas.ac.uk/icd/gjma/sam.html).

Table 3.1 lists the correlations between transport calculated between GRACE and ECCO OBP data and the two different SAM indices, as well as the SAM indices themselves. All are based on the low-frequency signal, with the trend removed. The correlations between both of the SAM indices and ECCO and GRACE calculated transports are high. GRACE correlates the most with the JISAO index (0.72). ECCO correlates highly with both the JISAO index (0.83) and NERC index (0.81). While the correlations are high between the indices and transport calculated, there are still some discrepancies among the time series. Figure 3.4 shows the low-frequency transport variability calculated from GRACE OBP, along with the low-frequency time series of the SAM with the trends removed. The trend was removed from the SAM indices and transport variability from GRACE to better observe other low-frequency signals. The SAM indices are slightly out of phase with the GRACE transport time series and with each other, which explains some of the lower correlations between GRACE calculated transport and the two SAM indices. Moreover, the correlation is higher after 2006 when SAM fluctuations are higher.

The SAM or AAO indices are only a proxy for wind variability over the Southern Ocean, will not completely represent potential local wind variations that may affect the low-frequency transport variability at the Australia-Antarctica choke point. Previous studies have examined the relationship between the SAM index and high-frequency transport variability at the Drake Passage (e.g., *Meredith et al.*, 2004; *Bergmann and Dobslaw*, 2012), however little work has been done to quantify the correlation between low-frequency transport variability of the ACC and the low-frequency, local winds.

Table 3.1: Correlations between transport (ECCO and GRACE) and the two SAM indices (JISAO and NERC).

	Correlation
JISAO/NERC	0.95
ECCO/GRACE	0.50
GRACE/JISAO	0.72
GRACE/NERC	0.66
ECCO/JISAO	0.83
ECCO/NERC	0.81

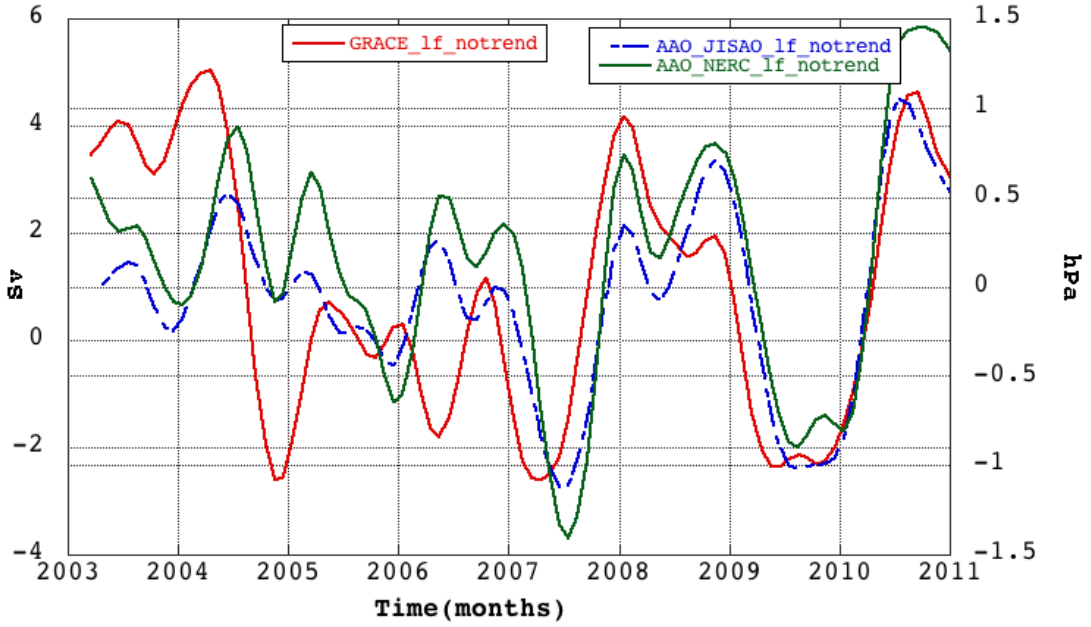

Figure 3.4: Time series of low-frequency transport variability, averaged between 125°E-155°E using GRACE OBP (red) and and low-frequency, with trend removed Southern Annular Mode Index from JISAO (blue), and NERC (green) with trend removed.

3.3 Analysis of Australia-Antarctica Transport and Southern Ocean Winds

The relationship between transport variability of the ACC and the Southern Hemisphere winds is of interest for understanding climate change. Due to the different hypotheses of how the ACC transport will react to a change in SH winds, we look at potential changes in transport variability calculated from GRACE OBP data at the Tasmania-Antarctica choke point and the coherency between zonal wind stress, as well as wind-stress curl.

We use the Cross-Calibrated Multi-Platform (CCMP) ocean surface winds monthly data Level 3.5A (http://podaac.jpl.nasa.gov/DATA_CATALOG/ccmpinfo.html; *Atlas et al.* (2008)). The time-series for each 1°x1° grid of unfiltered/unsmoothed zonal wind stress data was cross correlated with the time-series of the average transport variability calculated from GRACE OBP between 125°E-155°E (Figure 3.5). From this figure it is apparent that there is a high, significant correlation between the zonal wind stress and transport variability north of the Sub-Tropical Front; this is mainly related to the seasonal winds and variation in transport.

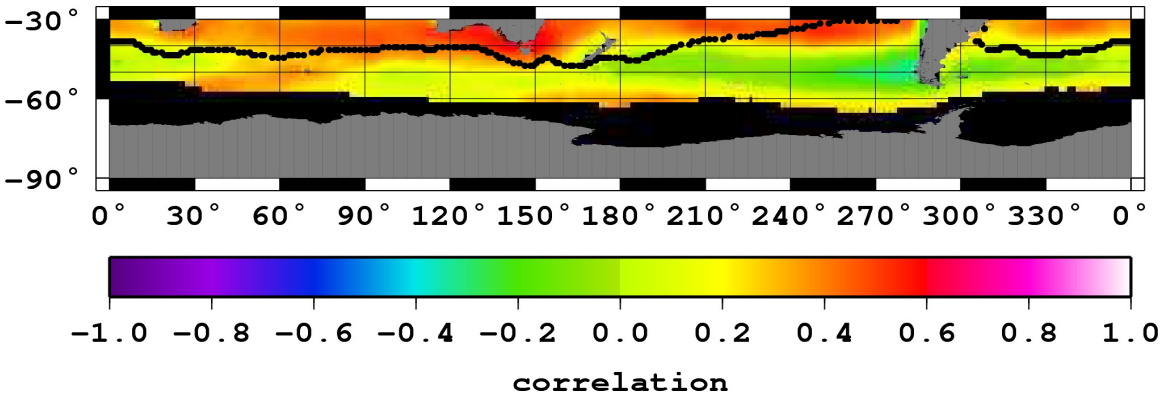

Figure 3.5: Map of correlation between zonal wind stress and transport. Transport is average transport between 125°-155° averaged over 2003-2011 and is correlated with each 1°x1° (2003-2011) zonal wind stress. The black line denotes position of the Sub-Tropical Front from *Orsi et al.* (1995).

After applying the low-pass filter to the zonal wind stress data, the data are correlated with the similarly low-pass filtered transport time series (Figure 3.6). There are significant, positive correlations south of the Sub-Tropical Front (shown in black), related to the Southern Annular Mode. Note the stronger, negative correlation (-0.6 to -0.8) just north of the STF in the Indian Ocean west of Australia. Winds north of the front are easterly (blowing to the west), while winds south of the front are westerly. This negative/positive correlation is suggestive of strengthening/weakening of the gradient between these winds (and hence the wind stress curl). Such changes can cause variable mass convergence along the STF, leading to acceleration/deceleration of the transport.

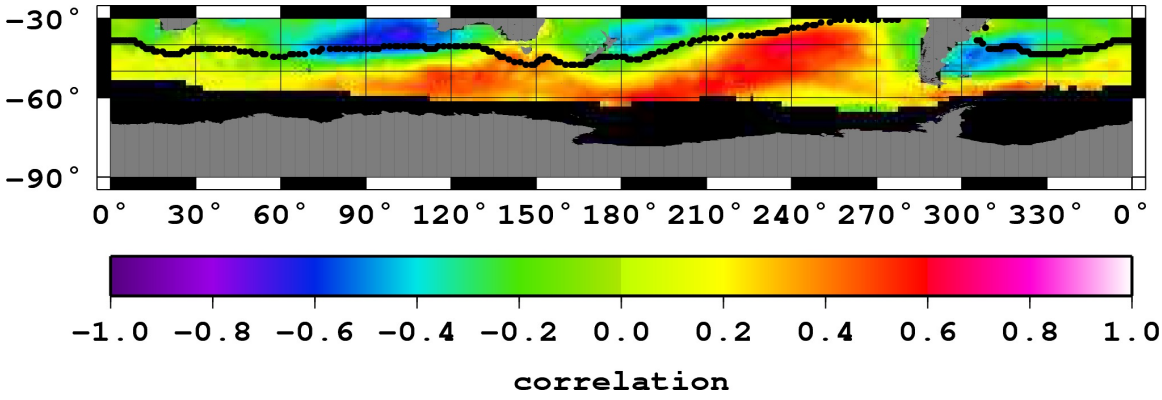

Figure 3.6: Map of correlation between low-frequency zonal wind stress and low-frequency transport. Transport is average transport between 125°-155° between 2003 and 2011 and is correlated with each 1°x1° time series of zonal wind stress. Both time series were low-pass filtered. The black line denotes the position of the Sub-Tropical Front from *Orsi et al.* (1995)

Wind stress curl (WSC) is defined as

$$WSC = (\frac{\partial \tau_y}{\partial x} - \frac{\partial \tau_x}{\partial y}) \tag{3.1}$$

Since winds in the Southern Ocean are zonally coherent, we can approximate this by

$$WSC \sim -\frac{\partial \tau_x}{\partial y} \tag{3.2}$$

The WSC was computed using the CCMP zonal wind stress data by computing meridional gradients via center-differences of the 1° gridded data.

There is no significant correlation between the unfiltered wind stress curl and ACC transport anywhere (Figure 3.7). However, after low-pass filtering, there are two regions of significant and high positive and negative correlation (Figure 3.8): between 60°E-90°E to the north of the STF (negative) and south of the front between 70°-120°E (positive). This is suggestive of changes in the convergence of mass at the STF due to wind stress curl variations.

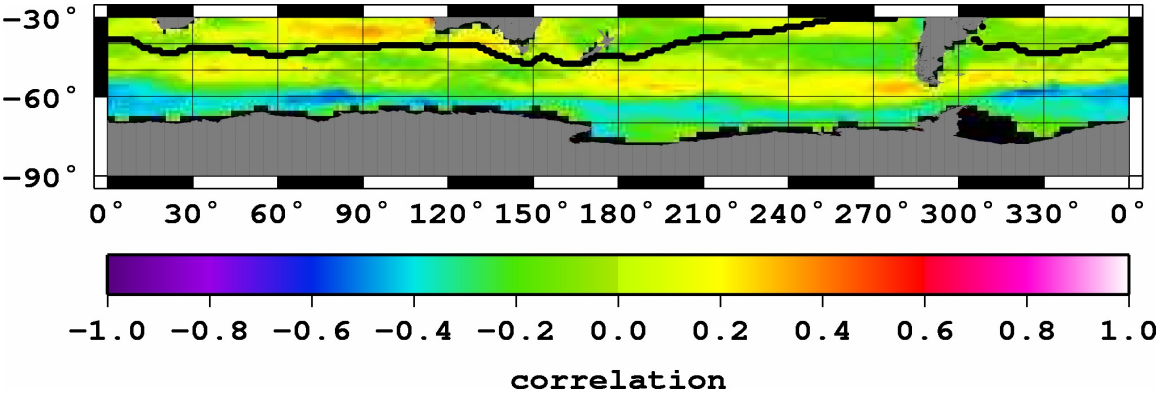

Figure 3.7: Map of correlation between wind stress curl and transport. Transport is average transport between 125°-155° and is correlated with each 1°x1° time series of wind stress curl, both for 2003-2011. The black line denotes position of the Sub-Tropical Front from *Orsi et al.* (1995).

To highlight the correlations we average the wind stress curl (WSC) in the areas of high correlation in Figure 3.8, north and south of the STF, and compare each location to the GRACE low-frequency transport variability. Figure 3.9 shows the average wind stress curl north of the STF between 60°E-90°E and 35°S-40°S, compared with the choke point transport variability. The correlation is -0.70 which is significant at the 99% level. Figure 3.10 shows the average wind stress curl between 70°E-120°E, and south of the STF, compared with the low-frequency choke point transport. The correlation is 0.62, significant at the 99% level.

Differencing the north and south wind stress curl averages (north-south) is an

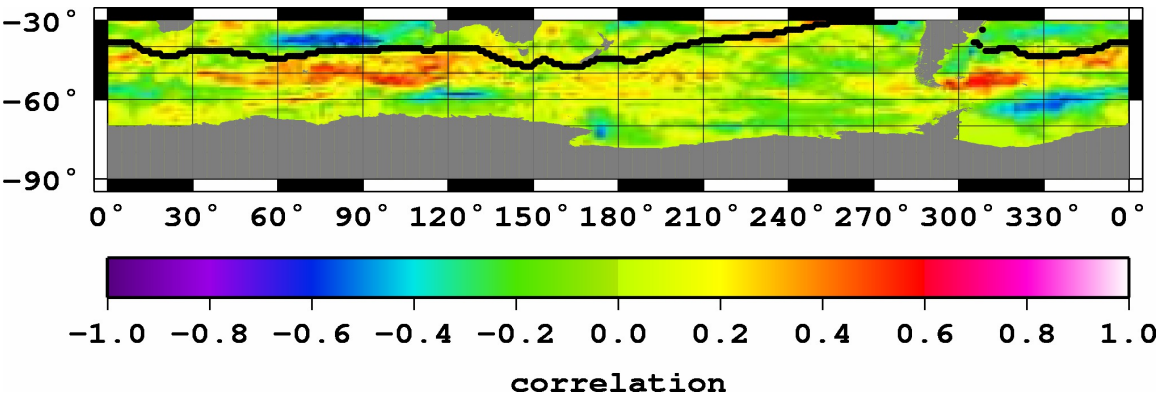

Figure 3.8: Map of correlation between low-frequency wind stress curl and low- frequency transport. Transport is average transport between 125°-155° and is correlated with each 1°x1° time series of wind stress curl, both for 2003-2011. Both time series were low-pass filtered. The black line denotes the position of the Sub-Tropical Front from *Orsi et al.* (1995)

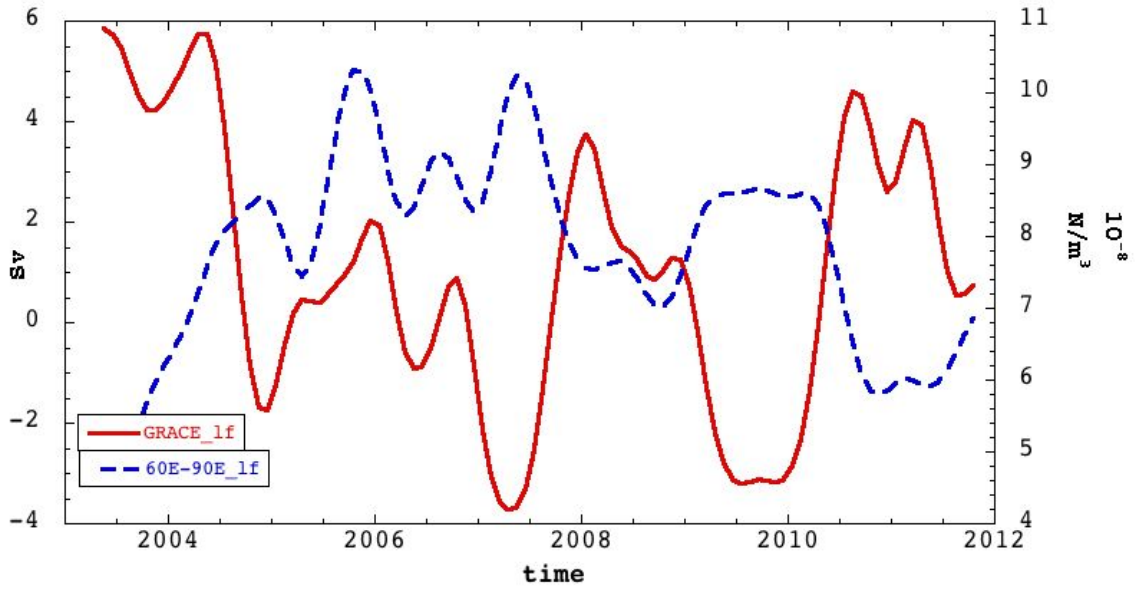

Figure 3.9: Time series of low-frequency wind stress curl north of the STF and low-frequency transport. Right axis (blue) is wind stress curl and left axis (red) is transport. Transport is average transport between 125°-155°.

approximation of the variable meridional gradient of WSC, which has been used in several studies to quantify variations in mass into and out of a region (e.g., *Chambers and Schröter*, 2011). When the WSC difference is compared to transport (Figure 3.11), we find that for low-frequencies, when the gradient between the north and

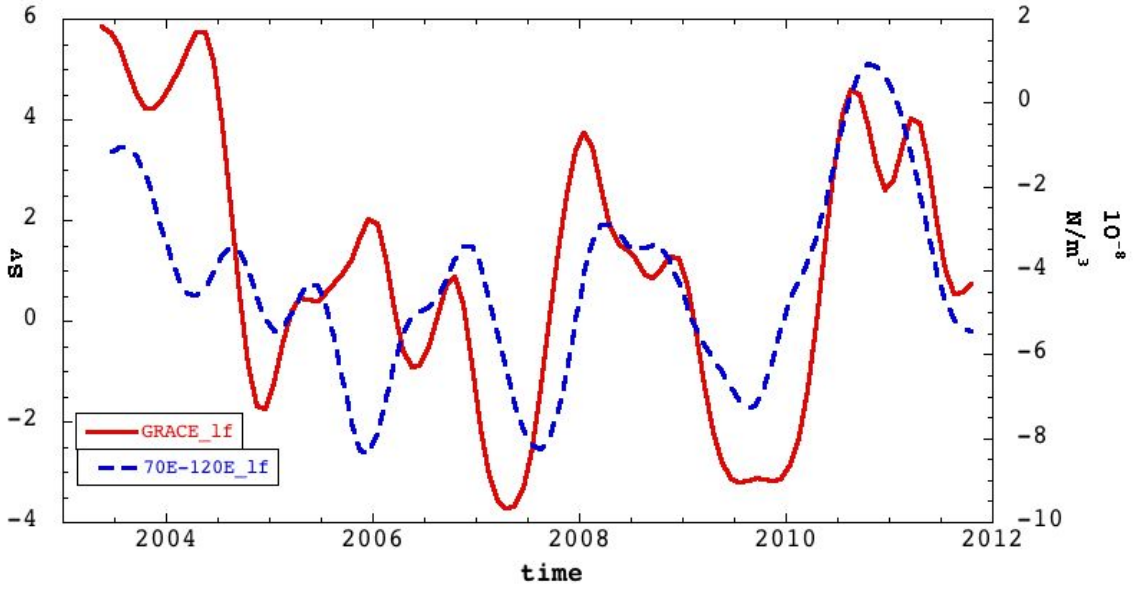

Figure 3.10: Time series of low-frequency wind stress curl south of the STF and low-frequency transport. Right axis (blue) is wind stress curl and left axis (red) is transport. Transport is average transport between 125°-155°.

south wind stress curl increases, the ACC transport decreases, and vice versa. The correlation is -0.69, significant at the 99% confidence level. In some areas this suggests that transport will increase to the east of the gradient. However, there are some periods where this is not the case, in fact the transport increases when the WSC difference increases (e.g., late 2005).

Sverdrup (1947) showed that the vertically integrated transport (M_y) directly related to wind stress curl by

$$M_y = \frac{1}{\beta}\left(\frac{\partial \tau_y}{\partial x} - \frac{\partial \tau_x}{\partial y}\right) = WSC, \tag{3.3}$$

Thus, the mean WSC north and south of the STF implied a meridional mass divergence, which must be replaced by an eastward transport of mass along the front. One might expect that if the divergence increases (indicated by increasing WSC difference in Figure 3.11) the transport measured by GRACE would also increase.

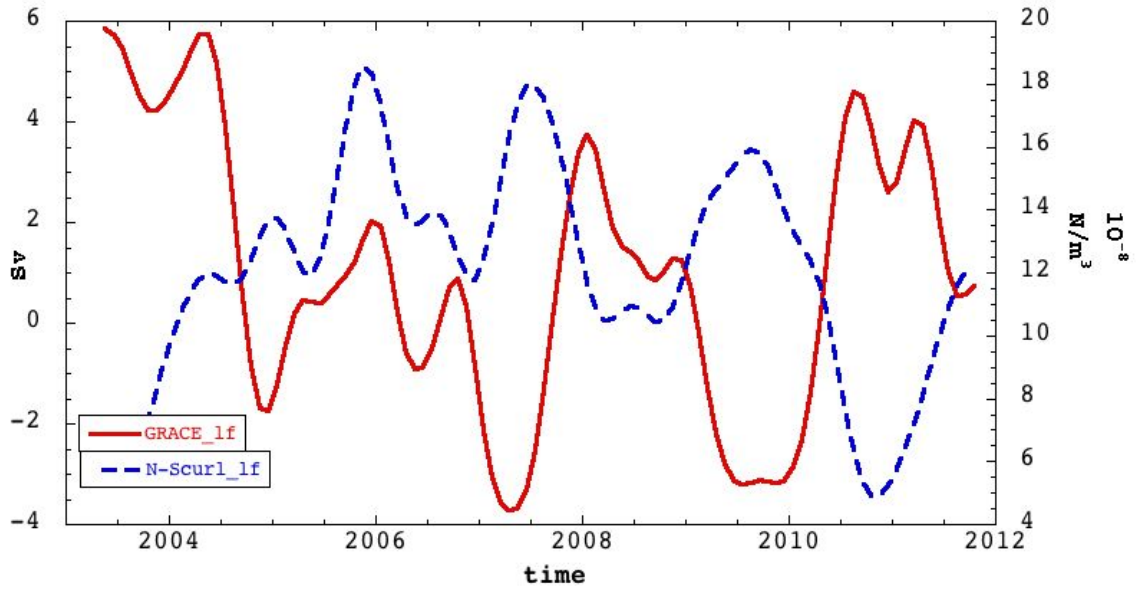

Figure 3.11: Time series of low-frequency wind stress curl difference between north and south of the STF and low-frequency transport. Right axis (blue) is wind stress curl and left axis (red) is transport. Transport is average transport between 125°-155°.

This, however, is not the case.

There are several explanations for this. First, the Sverdrup transport is only part of the total transport of the Southern Ocean (*Mestas-Nuñez et al.*, 1991). Since the transport is correlated with the SAM and other modeling studies (e.g., *Meredith et al.*, 2011) have linked the zonal wind changes associated with the SAM to ACC transport. The WSC changes in the Indian Ocean, because they are anti-correlated with the SAM, may slightly dampen the transport to what it would be with only forcing by the Southern Annular Mode.

Moreover, from the continuity equation

$$\frac{\partial M_{\mathrm{x}}}{\partial x} + \frac{\partial M_{\mathrm{y}}}{\partial y} = 0 \tag{3.4}$$

the gradient of M_{y} (or $\sim$ north-south WSC difference) leads to a gradient of zonal transport, meaning transport to the west of the high WSC area should vary differently

than transport to the east, or our study area.

When transport from the ECCO model and GRACE is examined between the STF and SACCF between 15°E and 45°E and compared to integrated transport variations south of Australia (Figure 3.12) it is clear both data observe significant differences in transport on either side of the region of highly variable WSC.

Thus, there is likely a more complicated relationship between ACC transport variability south of Australia than what has been assumed at the Drake Passage, most likely due to variations along the STF. Testing this idea is beyond the scope of this project, but warrants further investigation, like requiring a climate model, or a general ocean circulation model.

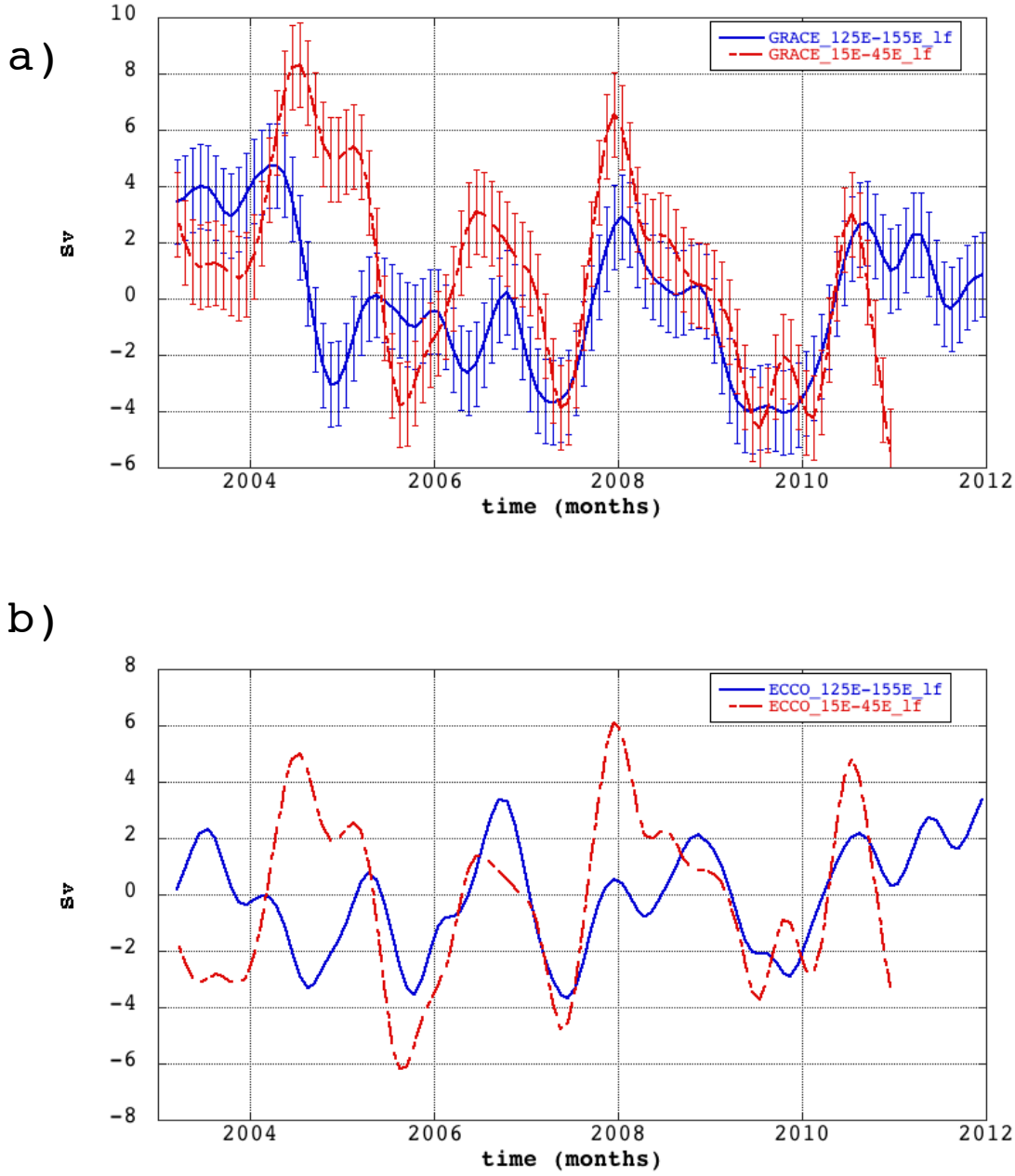

Figure 3.12: Time series of low-frequency transport calculated from GRACE and ECCO OBP east and west of the area of the wind stress curl gradient. Transport is average transport between 125°-155° (east) and 15°E-45°E (west).

Chapter 4

Conclusions and Future Work

Based on the results from the error analysis in Chapter 2, we have demonstrated that GRACE can observe variations in the Antarctic Circumpolar Current transport variability at spatial scales significantly smaller than assumed in previous studies. Instead of having to average over an entire ocean basin, we have been able to measure transport variability over only 30° longitude with lower uncertainty. We have quantified the uncertainty on monthly estimates and the trend uncertainty at the 90% confidence interval to be 3.96 Sv unfiltered and 1.5 Sv at the low frequency. From the spatial averaging analysis we focus our evaluation of transport variability to the area south of Australia from 125°E-155°E.

The trend we estimate from GRACE calculated transport variability is not significant at the 90% confidence interval and therefore we find no evidence of an acceleration in the overall transport at the Australia-Antarctica choke point during the time period between 2003-2011.

In Section 3.2 we discussed the correlation between the transport variability and the Southern Annular Mode at low frequencies. Evidence from other studies have suggested that there is a high correlation between the SAM and the transport through the Drake Passage. Our results are therefore consistent with the hypothesis that the SAM drives a significant portion of the transport variability of the ACC. In Section 3.3, we discussed an intriguing correlation with wind stress curl in the south

Indian Ocean, which suggested the possibility of local forcing of transport variability. This wind stress curl gradient, based on basic Sverdrup dynamics, would result in a meridional divergence of mass that must be balanced by a zonal convergence. We do find significantly different transport variations to the west and east side of this variable divergence region, but our observations are too limited to fully study the mechanisms relating the wind stress curl to transport variability in the region. Future studies will focus on understanding the relationship between the zonal winds (local, regional, and basin-averaged), wind stress curl, and how these are balanced in this region. In particular, we will study how coherent variations are in the ACC transport from one region to another, and how they may relate to local wind forcing.

As shown by this study there is still a great deal to understand about the dynamics and the forcing that drive the Antarctic Circumpolar Current. With the availability of new data sets, such as satellite gravimeter data from GRACE, we will be able to continue to work towards gaining a background understanding of such an important feature of the Southern Ocean and it's role in a variable climate.

Chapter 5

References

Amante, C., and B. W. Eakins (2009), *ETOPO1 1 arc-minute global relief model: procedures, data sources and analysis*, US Department of Commerce, National Oceanic and Atmospheric Administration, National Environmental Satellite, Data, and Information Service, National Geophysical Data Center, Marine Geology and Geophysics Division.

Atlas, R., J. Ardizzone, and R. N. Hoffman (2008), Application of satellite surface wind data to ocean wind analysis, in *SPIE*, edited by P. E. Ardanuy and J. J. Puschell, pp. 70,870B–70,870B–7, doi:10.1117/12.795371.

Bergmann, I., and H. Dobslaw (2012), Short-term transport variability of the Antarctic Circumpolar Current from satellite gravity observations, *Journal of Geophysical Research*, *117*(C5), C05,044, doi:10.1029/2012JC007872.

Bettadpur, S. (2007), Gravity Recovery and Climate Experiment Level-2 Gravity Field Product User Handbook, *Tech. rep.*, Center for Space Research, University of Texas Austin.

Bonin, J., and D. Chambers (2013), Uncertainty estimates of a GRACE inversion modelling technique over Greenland using a simulation, *Geophysical Journal International*, *194*(1), 212–229, doi:10.1093/gji/ggt091.

Bonin, J. a., and D. P. Chambers (2011), Evaluation of high-frequency oceanographic signal in GRACE data: Implications for de-aliasing, *Geophysical Research Letters*, *38*(17), n/a–n/a, doi:10.1029/2011GL048881.

Böning, C., A. Dispert, and M. Visbeck (2008), The response of the Antarctic Circumpolar Current to recent climate change, *Nature*, *1*(12), 864–869, doi:10.1038/ngeo362.

Chambers, D. P., and J. a. Bonin (2012), Evaluation of Release-05 GRACE time-variable gravity coefficients over the Ocean, *Ocean Science Discussions*, *9*(3), 2187–2214, doi:10.5194/osd-9-2187-2012.

Chambers, D. P., and J. Schröter (2011), Measuring ocean mass variability from satellite gravimetry, *Journal of Geodynamics*, *52*(5), 333–343, doi: 10.1016/j.jog.2011.04.004.

Cunningham, S., S. Alderson, B. King, and M. Brandon (2003), Transport and variability of the Antarctic circumpolar current in drake passage, *Journal of Geophysical Research*, *108*(C5), 1–17, doi:10.1029/2001JC001147.

Deacon, G. E. R. (1937), The hydrology of the Southern Ocean, *Discovery Reports*, *15*, 1–124.

Fukumori, I. (2002), A partitioned Kalman filter and smoother, *Monthly Weather Review*, (1999), 1370–1383.

Fyfe, J., and O. Saenko (2006), Simulated changes in the extratropical Southern Hemisphere winds and currents, *Geophysical Research Letters*, *33*(6), 1–4, doi: 10.1029/2005GL025332.

Gille, S., D. Stevens, R. T. Tokmakian, and K. Heywood (2001), Antarctic Circumpolar Current response to zonally averaged winds, *Journal of Geophysical Research*.

Graham, R., A. de Boer, K. Heywood, M. R. Chapman, and D. Stevens (2012), Southern Ocean fronts: Controlled by wind or topography?, *Journal of Geophysical Research*, *117*(C8), C08,018, doi:10.1029/2012JC007887.

Hallberg, R., and A. Gnanadesikan (2006), the structure and response of the wind-driven Southern Hemisphere overturning: Results from the Modeling Eddies in the Southern Ocean (MESO) project, *Journal of Physical Oceanography*, *36*(12), 2232–2252.

Hughes, C., M. Meredith, and K. Heywood (1999), Wind-driven transport fluctuations through Drake Passage: A southern mode, *Journal of Physical Oceanography*, *29*(8), 1971–1992.

Kim, S.-B., T. Lee, and I. Fukumori (2007), Mechanisms Controlling the Interannual Variation of Mixed Layer Temperature Averaged over the Niño-3 Region, *Journal of Climate*, *20*(15), 3822–3843, doi:10.1175/JCLI4206.1.

Lee, T., I. Fukumori, D. Menemenlis, Z. Xing, and L.-L. Fu (2002), Effects of the Indonesian throughflow on the Pacific and Indian Oceans, *Journal of Physical Oceanography*, *32*(5), 1404–1429.

Lovenduski, N. S. (2005), Impact of the Southern Annular Mode on Southern Ocean circulation and biology, *Geophysical Research Letters*, *32*(11), L11,603, doi: 10.1029/2005GL022727.

Marshall, G. (2003), Trends in the Southern Annular Mode from observations and reanalyses, *Journal of Climate*, *16*(24), 4134–4143.

Meredith, M., P. Woodworth, C. Hughes, and V. Stepanov (2004), Changes in the ocean transport through Drake Passage during the 1980s and 1990s, forced by changes in the Southern Annular Mode, *Geophysical Research Letters*, *31*(21), 1–5, doi:10.1029/2004GL021169.

Meredith, M., et al. (2011), Sustained monitoring of the Southern Ocean at Drake Passage: Past achievements and future priorities, *Reviews of Geophysics*, (2010), 1–36, doi:10.1029/2010RG000348.1.

Meredith, M. P., and A. M. Hogg (2006), Circumpolar response of Southern Ocean eddy activity to a change in the Southern Annular Mode, *Geophysical Research Letters*, *33*(16), L16,608, doi:10.1029/2006GL026499.

Mestas-Nuñez, A. M., D. B. Chelton, and R. A. De Szoeke (1991), Evidence of Time-dependent Sverdrup Circulation in the South Pacific from the Seasat Scatterometer and Altimeter, *Journal of Physical Oceanography*, *22*(8), 934–943, doi: 10.1175/1520-0485(1992)022¡0934:EOTDSC¿2.0.CO;2.

Munk, W. H., and E. Palmen (1951), Note on the Dynamics of the Antarctic Circumpolar Current, *Tellus*, *3*(1), 53–55, doi:10.1111/j.2153-3490.1951.tb00776.x.

Nowlin, W., and J. Klinck (1986), The physics of the Antarctic circumpolar current, *Reviews of Geophysics*, *24*(3), 469–491.

Orsi, A., T. Whitworth, and W. Nowlin (1995), On the meridional extent and fronts of the Antarctic Circumpolar Current, *Deep Sea Research Part I: Oceanographic Research Papers*, *42*(5).

Ponte, R. M., and K. J. Quinn (2009), Bottom pressure changes around Antarctica and wind-driven meridional flows, *Geophysical Research Letters*, *36*(13), L13,604, doi:10.1029/2009GL039060.

Rintoul, S., and S. Sokolov (2001), Baroclinic transport variability of the Antarctic Circumpolar Current south of Australia(WOCE repeat section SR 3), *Journal of Geophysical Research*, *106*(C2), 2815–2832.

Saenko, O., J. Fyfe, and M. England (2005), On the response of the oceanic wind-driven circulation to atmospheric CO 2 increase, *Climate Dynamics*, *25*(4), 415–426, doi:10.1007/s00382-005-0032-5.

Sokolov, S., and S. Rintoul (2009), Circumpolar structure and distribution of the Antarctic Circumpolar Current fronts: 1. Mean circumpolar paths, *Journal of Geophysical Research*, *114*(C11), 1–19, doi:10.1029/2008JC005108.

Sverdrup, H. (1947), Wind-driven currents in a baroclinic ocean; with application to the equatorial currents of the eastern Pacific, *Proceedings of the National Academy of Sciences of ...*, *33*(11), 318–326.

Swenson, S., and J. Wahr (2006), Post-processing removal of correlated errors in GRACE data, *Geophysical Research Letters*, *33*(8), L08,402, doi: 10.1029/2005GL025285.

Tapley, B. D., S. Bettadpur, M. Watkins, and C. Reigber (2004), The gravity recovery and climate experiment: Mission overview and early results, *Geophysical Research Letters*, *31*(9), L09,607, doi:10.1029/2004GL019920.

Thompson, D., and J. Wallace (2000), Annular modes in the extratropical circulation. Part I: month-to-month variability*, *Journal of Climate*, *13*(5), 1000–1016.

Wahr, J., M. Molenaar, and F. Bryan (1998), Time variability of the Earth's gravity field: Hydrological and oceanic effects adn their possible detection using GRACE, *Journal of Geophysical Research*, *103*, 205–229.

Zlotnicki, V., J. Wahr, I. Fukumori, and Y. T. Song (2007), Antarctic circumpolar current transport variability during 2003-05 from GRACE, *Journal of Physical Oceanography*, *37*(2), 230–244, doi:10.1175/JPO3009.1.